Diploma Thesis

Acoustic modelling of perforations in automotive exhaust mufflers using 3D cells

Author: Jan Bräuer

Institute for Internal Combustion Engines and Thermodynamics

Graz University of Technology

and

AVL List GmbH

Assessor : Ao.Univ.-Prof. Dipl.-Ing. Dr.techn. Hans-Herwig Priebsch

Supervisors : Dr. Robert Fairbrother

Dipl.-Ing. PhD Andreas Dolinar

Graz, June 2011

EIDESSTATTLICHE ERKLÄRUNG

Ich erkläre an Eides statt, dass ich die vorliegende Arbeit selbstständig verfasst, andere als die angegebenen Quellen/Hilfsmittel nicht benutzt und die den benutzten Quellen wörtlich und inhaltlich entnommenen Stellen als solche kenntlich gemacht habe.

Graz, am ....

(Unterschrift)

STATUTORY DECLARATION:

I declare that I have authored this thesis independently, that I have not used other than the declared sources / resources, and that I have explicitly marked all material which has been quoted either literally or by content from the used sources.

....

date (signature)

Abstract

The acoustic prediction of automotive exhaust systems is an important aspect to shorten development time and to find compromises between good acoustic damping characteristics and low flow resistance for optimal engine performance. One dimensional solutions already provide very good results but have some disadvantages, e.g. the limiting accuracy in predicting higher order mode effects and the modelling of complex muffler geometries is hard to accomplish. Therefore the approach of using 3D cells for acoustic and performance prediction was recently introduced.

Perforated pipes and plates in exhaust muffler systems are commonly used to enhance the acoustic performance and to keep the back pressure low. The aim of this thesis is to extend the 3D cell approach with a "perforated connector" for modelling perforated pipes and plates. Therefore, a finite volume based approach is used to develop a model for the "perforated connector". For testing and verification purposes this model is implemented in the AVL Boost code. To verify the solution, and to identify appropriate values for the influencing parameters, measurements are compared with simulation results for different muffler types.

The investigations show that the functionality of the implemented model tends toward reasonable results but also that the 3D cell method can be further improved in order to achieve more accurate predictions.

Kurzfassung

Die Möglichkeit, das akustische Verhalten von Auspuffschalldämpfern vorherzusagen, ist ein wichtiger Aspekt um Entwicklungszeiten zu verkürzen und einen Mittelweg zwischen guten akustischen Eigenschaften und geringem Strömungswiderstand für möglichst gute Motorleistung zu finden. Eindimensionale Simulationsmodelle bieten bereits sehr weit entwickelte Lösungen, haben aber einige Nachteile, so ist z.B. die Genauigkeit der Vorhersage von Moden höherer Ordnung beschränkt, und komplexe Geometrien sind oft recht umständlich zu modellieren. Deshalb wurde eine dreidimensionale Lösung entwickelt, welche 3D Zellen für die akustische Simulation verwendet.

Perforierte Rohre und Platten werden vielfach zur akustischen Verbesserung in Auspuffschalldämpfern verwendet, während auch der Gegendruck recht gering ist. Das Ziel dieser Diplomarbeit ist es für die 3D Zellen eine "perforierte Verbindung" zu entwickeln, um Perforationen in Rohren und Platten modellieren und simulieren zu können. Im Zuge dieser Arbeit wurde daher das verwendete Finite Volumen Verfahren erweitert um eine "perforierte Verbindung" modellieren zu können. Um das Verfahren zu testen und verifizieren ist es in den AVL Boost Code implementiert worden. Um die passenden Werte für die Parameter, welche die Ergebnisse beeinflussen, zu finden, werden Simulationsergebnisse mit Messergebnissen für verschiedene Schalldämpfertypen abgeglichen.

Die Untersuchungen zeigen, dass die Funktionalität des implementierten Modells gegeben ist, aber auch, dass die 3D Zellen Methode weiter verbessert werden kann um genauere Simulationsergebnisse zu erhalten.

Contents

1 Introduction

1.1 Motivation and objective

To investigate acoustic behaviour and performance of exhaust muffler systems, measurements and computer simulations can be done. Compared to measurements which are of great effort, simulation methods provide fast and accurate prediction. One dimensional models such as BOOST Linear Acoustics [1], which is based on the program SID (Sound in Ducts) developed in the 1980s [2], are limited in predicting higher order mode effects due to the assumption of plane wave propagation. Furthermore fundamental knowledge of acoustically equivalent systems is necessary which also implies the consideration of artificial end corrections for pipe ends or abrupt area changes (cf.[3] and [4]). Those solvers are very useful for simple models and their advantage is the very fast computational time.

As computational power has become cheaper over the last few decades and the accuracy of one dimensional simulation tools is limited, a quasi three dimensional approach is further investigated. Therefore a generic 3D cell for the acoustic modelling of intake and exhaust systems is developed [4]. Due to the 3D nature of these models it is also possible to predict higher order modes and improve the accuracy of models at higher frequencies [4]. In this work the emphasis is on the modelling of perforated pipes and plates. Hence a perforated connector which connects two or more 3D cells is developed. To verify the solution simulations of transmission loss and pressure loss of different muffler types which contain perforated pipes are compared to measurements and plane wave approaches.

The impedance of the perforation is caused by friction and inertia. Those effects are accounted for by parameters, where the objective is to find values which are valid for all different muffler configurations, and for simulations with mean flow and without mean flow.

1.2 Literature review

Frequency domain approaches and time domain approaches have to be distinguished. Research on theory models of perforated pipe mufflers have been done by several authors over the past few decades. A short review is given in this chapter.

1.2.1 Frequency domain approaches

In order to predict the acoustic behaviour of exhaust mufflers with perforated pipes in the frequency domain there are mainly two approaches which are the *continuous method* also called *distributed parameter method* [5][6][7][8][9] and the *discrete method* also called *segmentation method* [10][11][12].

Due to their closed form solutions both approaches require very short computational time but are limited to muffler types with very simple geometry.

Continuous method The continuous method or distributed parameter method is based on the one dimensional equations for conservation of mass and momentum. Solving this equations leads to the parameters of the transfer matrix, which are needed for the calculation of the transmission loss. This method uses surface averaged wall impedance (cf. [13]). In 1978 Sullivan and Crocker [5] did the first research on this method, but their model does not take into account flow through the perforation and it is limited to concentric through flow mufflers only.

Further investigations and improvements on this method were made e.g. by Jayaraman and Yam [6] in 1981, Munjal et al. [7] in 1986, Peat [8] in 1987, Dokumaci [9] in 1996 and Davies et al. [14] in 1996. The distributed approach is mainly convenient for relatively simple perforated mufflers [13].

Discrete method The discrete method, also called segmentation method was first established by J. W. Sullivan [10] [11] in 1979. This approach separates the whole chamber into segments in the axial direction. Each segment is described by a separate transfer matrix. The total transfer matrix of the perforated element is found by successive multiplication of the transfer matrices of each element.

Further research and newer versions of the segmentation approach has been done by Dokumaci [15] in 2001 and T. Elnady and M. Åbom [13] in 2004.

1.2.2 Time domain approaches

There are some general methods for calculating fluid flow through engine manifolds with those it is possible to predict the acoustical and performance behaviour. The following outline is mainly taken from J.H.Ferziger "Computational Methods for Fluid Dynamics" [16].

Until the mid 1980s the *mesh method of characteristics* was the dominant numerical technique when it was displaced my modern finite difference schemes due to the greater accuracy and robustness of the latter (cf.[17][18]). The method of characteristics is a first order method and its intrinsically dissipative character produces an undesired high frequency filtering effect which may be unimportant for performance studies, but clearly affects its suitability for noise prediction (cf.[19][20]).

The *finite difference method* is the oldest method for numerical solution of partial differential equations, believed to have been introduced by Euler in the 18th century [16]. It is the easiest method for simple geometries but that is also its main disadvantage. Usually this method has been applied to structured grids where it is very simple and effective.

The *finite volume method* is the most used method in CFD codes (computational fluid dynamics) which is also why the proposed modelling on the perforated intersection between 3D cells is based on it (see chapter 3). In contrary to the previous method it can handle any type of grid, so also complex geometries are possible. Another advantage is that this method is relatively simple to understand and to program.

Another very popular method is the *finite element method* which uses an unstructured grid that makes it more difficult to find efficient solution methods. The distinguishing feature of finite element methods is that the equations are multiplied by a weight function before they are integrated over the entire domain [16]. The ability to handle complex geometries is more advanced compared to other methods. A combination of finite volume and finite element method would be a hybrid method, the so called control volume based finite element method.

Impedance modelling for time domain solvers

For calculating the fluid flow through perforations no universal applicable numerical method exists. Hence it has to be adopted for the particular finite method used. For one dimensional solvers two very similar methods are briefly described here.

In 1997 Onorati [21] proposed a method which is based on the finite difference method for a one dimensional solution. Each hole through the perforation is modelled using a short pipe with the same diameter and length as the equivalent hole diameter and wall thickness of the perforated pipe. A through flow muffler with a perforated pipe is shown in figure 1(a), where the proposed equivalent system is seen in figure 1(b).

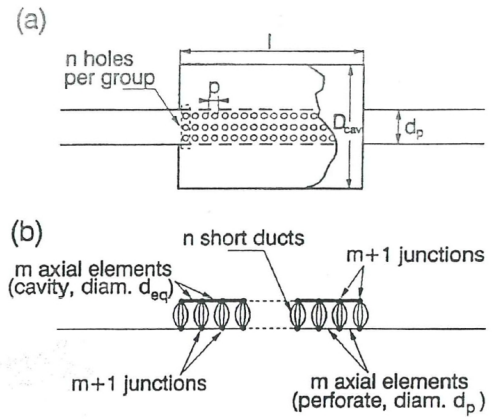

Figure 1 – (a) Schematic of a typical perforated pipe surrounded by a cavity liner; (b) sketch of the duct system adopted for the simulation [21].

The holes of the perforated pipe are aligned in circles, where p is the spacing to the next circle of holes. The number of holes n of one circle is represented by n very short ducts which connect the perforated volume with the surrounding cavity volume. Both volumes are divided by $m = l/p$ elements with length p. The perforate pipe has d_p as its diameter and the cavity an equivalent diameter of d_{eq} calculated from $d_{eq}^2 = D_{cav}^2 - d_p^2$.

The method used by Onorati is a non-linear gas dynamic approach. The flow in every single hole of the perforation is considered by branches of several ducts using the equal total enthalpy (constant pressure) model. For saving computational time several holes are summed up to reduce the number of ducts while the porosity level remains the same.

In 2003 A.I. Abd El-Rahman et al. [22] used a model based on the method of characteristics, while the perforation model follows that proposed by Onorati [21] with only slight differences. In the case of zero mean flow and low pressure level for the acoustic excitation he found the dissipative effect less significant therefore the behaviour would be predominately reactive. Tested are through flow mufflers, which means that mainly grazing flow is considered. El-Rahman found different values for the end correction coefficient. For long resonators $\alpha = 0.8$ and for for short resonators $\alpha = 0.7$, both with low porosities between 2 % - 5 %.

G. Montenegro et al. [23] recently introduced a numerical approach to model perforated elements which uses the finite volume method for a 3D cell approach, which is the only proposed method in this context at present. This approach is described in chapter 3.2 and used for the simulation models in chapter 4.

1.3 Proceeding and structure of the work

First the numerical method from G. Montenegro et al. [23] for the perforation was adopted for the implementation in the Boost code. This required the use of the programming language Fortran which is commonly used for numerical computation. Than a series of experimental trials to achieve usable results was carried out where finally several simulation results for different muffler types have been compared to measurements.

After description of the objectives and motivation of the present thesis and a short overview on existing literature in chapter 1, here the structure is briefly clarified.

Basic theory about sound propagation in exhaust mufflers is covered in chapter 2 where also the theory on acoustic impedance of perforations and its influencing factors are described. Chapter 3 contains a brief overview about the finite volume method which is used for the modelling of the mufflers volume and a detailed description how the modelling of the perforation is implemented.

In chapter 4 several 3D cell meshes with different mesh sizes for different muffler types were generated and first results for the transmission loss are accomplished. The investigated muffler types namely are a through flow muffler with short and long chamber, a

single plug, double plug and eccentric plug muffler, and further a two chamber eccentric plug muffler with a more complex geometry. The achieved results have some deviations, but basically deliver good agreement with measurement results. In chapter 5 the accomplished results are summarized and a short outlook on further investigations is given.

1.4 Summary of the results

The investigations accomplished in the course of this thesis, where several parameters are studied, show the following relations. The smaller the 3D cell size the more accurate are the simulation results of the transmission loss. Because the 3D cell mesh is coupled with a 1D pipe which uses a different solver but the same time step, the cell size of the 1D pipe also effects the accuracy of the simulation results.

The model of the perforated impedance has two parameters which are the friction factor and the end correction length coefficient. Simulation results of the transmission loss for plug mufflers, where the flow is forced through the perforations, require higher friction factors compared to muffler types where the flow is mainly grazing the perforations. The variation of the end correction coefficient causes a frequency shift of higher order peaks but this coefficient was kept constant for all simulation results.

2 Sound propagation through exhaust mufflers

In this chapter at first the origin of the sound noise is clarified. How sound attenuation is achieved in exhaust mufflers is explained in the the second subchapter followed by the explanation of the impedance of perforations in subchapter 2.3 . Subchapter 2.4 covers the effect of higher order modes and in subchapter 2.5 commonly used methods for measuring sound attenuation are described.

2.1 Where the sound comes from

The sound of a vehicle is mainly composed of the following components:

- noise of the engine/aggregates (e.g. engine, gearbox, fan)
- noise of the exhaust gas system
- noise of the intake system
- sound of the tire and road noise
- sound caused by flow around the vehicle

Concerning the IC-engine the sound source can be further divided into sound originated from combustion, mechanics and flow [24][25]. In this work the sound originated from combustion and flow is of interest. The actual mechanism behind the combustion sound is the very fast pressure fluctuations. Very high pressure shock waves are caused by expansion of the compressed gas in the combustion chamber when the valve opens. The dominating noise component is always at the same frequency as the firing frequency. The number of cylinders divided by two results in the dominating engine order. That means for a four cylinder engine the second order is the dominating whereas for a six cylinder engine the third order is the dominating [26]. However the noise generated consists mainly of the firing frequency and its first few harmonics.

In general the propagating sound wave through an exhaust muffler consists of two components. First the generated shock waves which for its impulsive character has a broad band spectrum and second the mean flow through the system which also has a broad

band spectrum but up to 10 kHz (cf.[26]). The combination of both components is called *unsteady mean flow*.

2.2 Exhaust mufflers

The exhaust system of an automotive IC engine has several demands which need to be fulfilled. Mainly it conveys the burnt gases from the combustion chamber through different sections of the system. As seen in figure 2 this system usually consists of a catalyst which reduces the toxic exhaust emissions and the front, middle and rear silencer whose primary purpose is noise reduction, but also give some potential for sound design. For small cars and utility vehicles often a combined system is used as seen in figures 3 and 4. A major demand is to damp the propulsion exhaust noise while keeping the back pressure low for best engine performance.

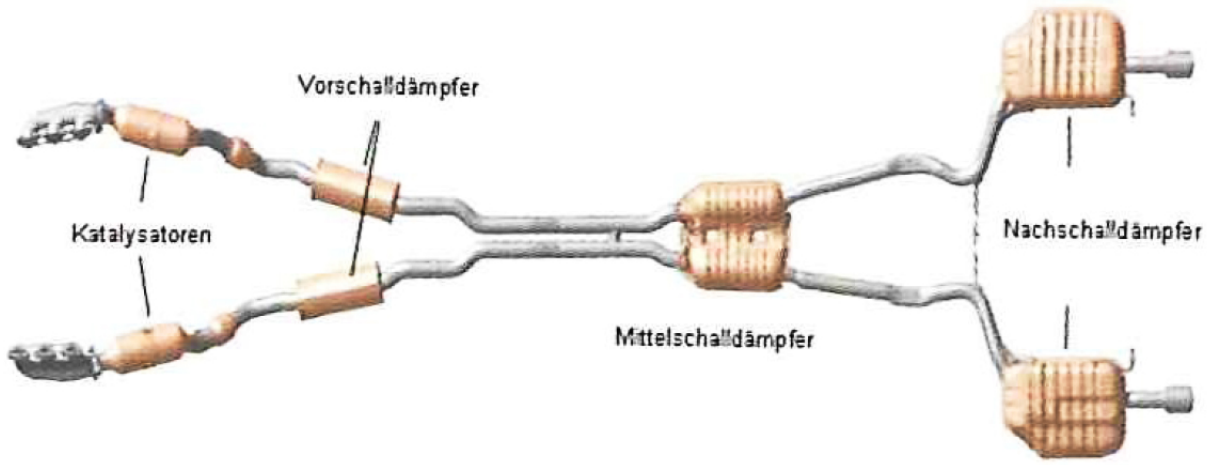

Figure 2 – Double flow exhaust system [26]: f.l.t.r.: catalyst, front silencer, middle silencer, rear silencer

The challenge is to design a muffler which handles both demands in an acceptable range while considering limitations in space and weight. The two principles which are *reactive* and *dissipative* sound attenuation generally are combined in conventional exhaust systems. Such a *hybrid muffler* as seen in figure 5 consists of several separated volumes, which are connected through closed pipes, perforated pipes or perforated plates.

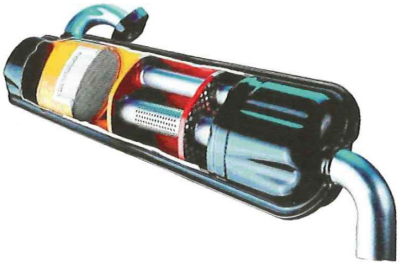

Figure 3 – Muffler with integrated catalyst for compact cars

Figure 4 – Integrated system for utility vehicles

Dissipative sound attenuation comes into account when the exhaust gas flows through absorption material. The air flow causes friction in the material where the acoustic sound energy is dissipated into thermal energy. Absorptive materials such as mineral wool, carbon fiber felt or steel wool are commonly used (cf. [26]). With this principle a broad band attenuation is achieved but it has its limitations at low frequencies.

Reactive sound attenuation can be used to attenuate low frequency noise. This is caused by sound reflection when the cross section area changes and therefore sound is reflected back to the sound source or within Helmholtz resonators which can be tuned to attenuate noise at certain narrow band frequencies. In an exhaust muffler usually several chambers with different dimensions are combined and connected with pipes which are often perforated pipes. Due to a simple expansion chamber is the basis of all commonly used exhaust mufflers it is described more in detail.

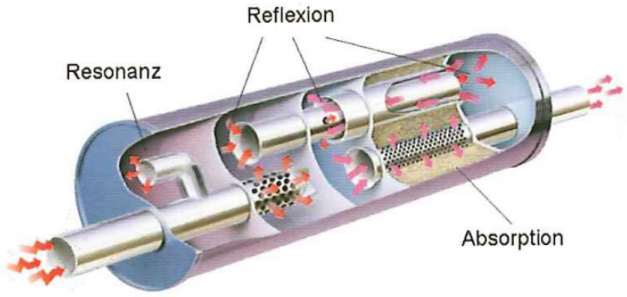

Figure 5 – Fictitious silencer with all damping principles: f.l.t.r.: resonance, reflection and absorption [26]

Such a simple expansion chamber is pictured in figure 6 with a typical characteristic curve of the transmission loss seen in figure 7 with maximums and minimums determined as follows:

$$f_{max} = \frac{nc}{4L}, \;\; n = 1, 3, 5 \qquad f_{min} = \frac{nc}{4L}, \;\; n = 2, 4, 6, \tag{2.1}$$

where the number n determines if its a minimum or maximum, c is the speed of sound and L the length of the chamber. It should be considered that the speed of sound is dependent on the temperature T as $c(T) \approx 331.3 + 0.6T$ [27] and therefore has influence on the propagating wave length. This causes a frequency shift when the temperature changes (compare with figure 42).

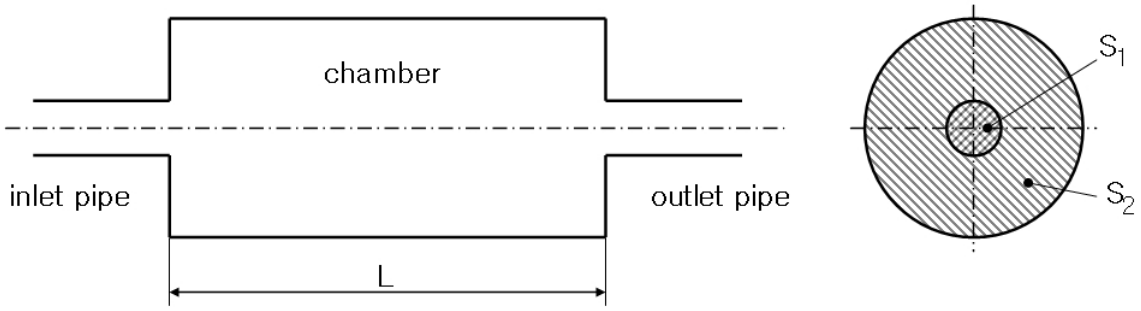

Figure 6 – Simple expansion chamber

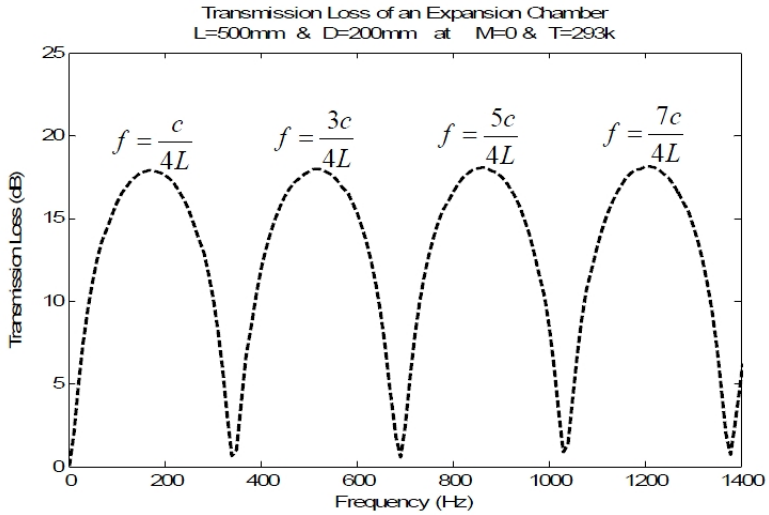

Figure 7 – Transmission loss of a simple expansion chamber [28]

The transmission loss without considering dissipation and assuming plane wave propagation can be calculated as follows (cf. [29]):

$$TL = 10 \log\Big[\frac{4\cos^2 kL + (m + m^{-1})^2 \sin^2 kL}{4}\Big], \tag{2.2}$$

where k is the wave number, L the length of the chamber and $m = S1/S2$ the ratio of cross section area of the inlet pipe to that of the chamber. For calculating the maximum of the transmission loss just the cross section area ratio is necessary (cf. [29])

$$TL_{max} = 10 \log\Big[\frac{(m + m^{-1})^2}{4}\Big], \tag{2.3}$$

so basically the strength of the damping is determined by the diameter, and the maximum frequencies f_{max} and minimum frequencies f_{min} are determinde by the length of the chamber.

Despite this very simple model, exhaust mufflers can be shaped in any arbitrary form. The shape is aligned to the engine and car concept, but the basic principle of sound attenuation for low frequencies remains the same and the characteristic curves for the transmission loss usually has similarities to that of a simple expansion chamber.

2.3 Perforated pipes

Perforated pipes are commonly used in silencers for automotive engines. Usually one or more perforated pipes are installed within an exhaust muffler. Often they connect the sections of a chamber and in a lot of applications the perforated pipe is for saving the absorptive material behind it and to influence the reactance and flow resistance.

Acoustic impedance of the perforation

The perforated pipe or perforated plate is a barrier for sound waves to propagate. This is referred as acoustic impedance. It is defined as the ratio of the acoustic pressure loss across the perforation to the normal particle velocity. For a single hole that is $Z_h = \frac{p_1 - p_2}{U_h}$, where the impedance is a complex quantity. The characteristic acoustic impedance of air is $Z_0 = \rho_0 c_0$ where ρ_0 and c_0 are the density and sound speed for air respectively.

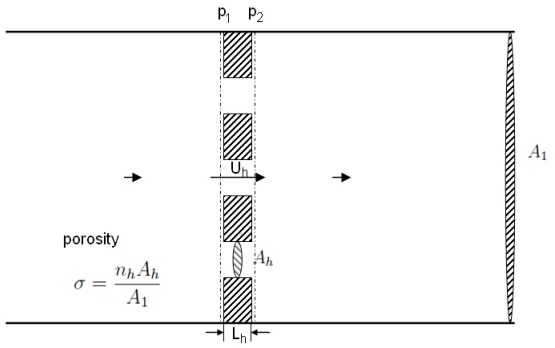

Figure 8 – Perforated plate in a duct

The dimensionless acoustic impedance of a hole is $\zeta_h = \frac{Z_h}{Z_0}$ which is in complex quantities written as:

$$\zeta_h = \frac{p_1 - p_2}{Z_0 U_h} = \frac{R_S + jk_0 L_S}{\rho_0 c_0} = R + jk_0 L_{C,h} \tag{2.4}$$

where p_1 and p_2 are the acoustic pressure before and after the plate, as seen in figure 8, U_h is the particle velocity in the holes, R_S and L_S the specific resistance and specific inertance. $L_{C,h} = L_h + 2\Delta l = L_h + \alpha d_h$ is the corrected hole length as seen in figure 9 where α is the end correction coefficient and d_h the hole diameter.

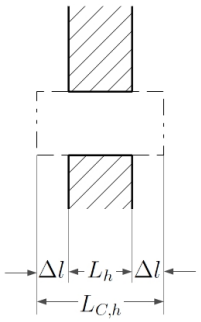

Figure 9 – Correction length

For the whole plate the dimensionless acoustic impedance is the impedance of a single hole divided by the porosity σ which is the ratio of the sum of all hole areas $\sum A_h$ to the total area A_1 as seen in figure 8:

$$\zeta_p = \frac{\zeta_h}{\sigma} \tag{2.5}$$

Sullivan and Crocker [5] found an empirical relationship for the acoustic impedance which is widely used:

$$\zeta_p = \frac{0.006 + jk_0(L_h + 0.75d_h)}{\sigma} \tag{2.6}$$

The value 0.75 is the end correction coefficient α. Some comparisons with other values are done in chapter 3.2. Unfortunately this very simple formula does not take into account all influencing factors which can affect the acoustic impedance. Generally it depends on the following influencing factors:

(1) constitution of the edges of the holes (sharp or rounded down)

(2) inertia, that is the attached mass in the holes of the perforation plus the appropriate correction mass

(3) interaction between holes (porosity σ, diameter of holes d_h)

(4) influence of mean flow through the holes or grazing the holes

(5) linear or non-linear regime

(6) discharge coefficient

The listed points are explained more in detail:

Points (1), (2) and (3): The constitution of the edges of the hole and the wall surface roughness influence the resistance which is the real part of the impedance. For time domain solvers this is usually accounted for with the friction factor. The inertia (reactance) is constituted as the volume of the holes plus an appropriate mass end correction which is augmenting this volume, which can be seen in figure 10(a). Also pictured in figure 10 is the interaction between holes which is affecting the resistance and reactance.

With porosities greater than 15-20 %, Davies [14] found that perforated tubes behave as if its walls are acoustically transperent.

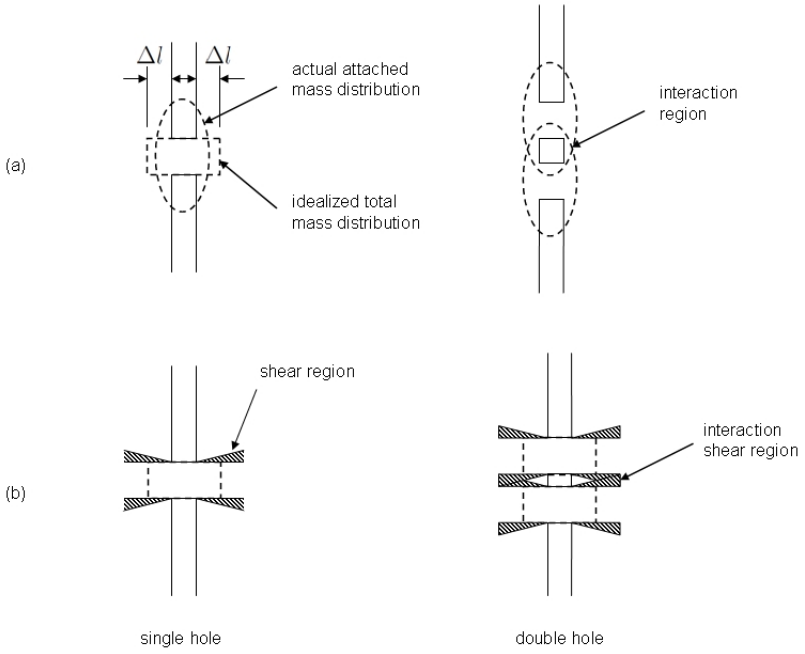

Figure 10 – Schemes for interaction effect: (a) for attached mass considering reactance and (b) shear region vs. reduced shear region where friction takes into account(cf. [30])

Point (4): In the presents of mean flow, whatever the structure of the perforation is, the resistance of the perforation tends to increase and the reactance tends to decrease (cf.[11]). Also observed is that the influence of through flow on the impedance is significantly smaller than that of grazing flow at the same Mach number (cf. [14]).

Also Elnady [31] confirms the influence of mean flow and describes the dependency on the grazing flow as follows: The flow blows away some of the end effects which result in a decrease of the so-called attached mass. This results in an increase of the acoustical resistance of the hole and a shift in the resonator resonance frequency. The orifice resistance increases with mean flow speed while the reactance decreases. Few purely theoretical predictions of the effects of grazing flow on orifice impedance have been attempted, probably because of the complexity of the problem [31].

Point (5): J.W. Sullivan [11] found that the perforated impedance is in the linear regime if the fluctuating velocity amplitude in the holes is less than about 2-3 m/s, in the absence of through flow. With grazing flow Mach number M<0.025, experimental evidence [10][11] suggests that the linear regime is maintained as long as the fluctuation pressure amplitude, expressed as a sound pressure level (SPL), remains less than 120-125 dB [14]. For the investigated examples in chapter 4 with Mach numbers between M=0.05-0.1 the perforated impedance has to be considered in the non-linear regime.

Point (6): The discharge coefficient C_d is a factor which is often considered in impedance models for perforations. It is related to the effect of *vena contracta* which is defined as the cross section where the contraction is greatest as seen in figure 11. It is defined as the product of the velocity coefficient C_v and the coefficient of contraction C_c:

$$C_d = C_v C_c \tag{2.7}$$

where $C_v = \frac{v_a}{v_t}$ is the ratio of actual velocity to theoretical velocity at the vena contracta and $C_c = \frac{A_2}{A_0}$ the ratio of the cross section area at the vena contracta to the cross section area at the orifice as seen in figure 11.

F. Payri et al. [32] investigated the discharge coefficient for dividing and combining flow for perforated pipes with a closed end. By use of a steady flow approach the pressure loss characterisation of perforated pipes for combining and dividing flow, as seen in figure 12, are investigated.

The effective discharge coefficient C_D is dependent on the porosity and hole diameter of the perforation and also on the ratio of the perforated area A_p to the cross section

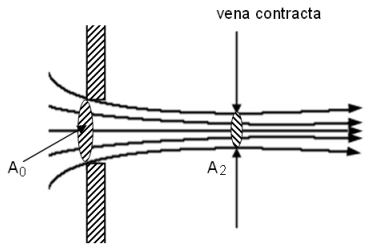

Figure 11 – Effect of vena contracta

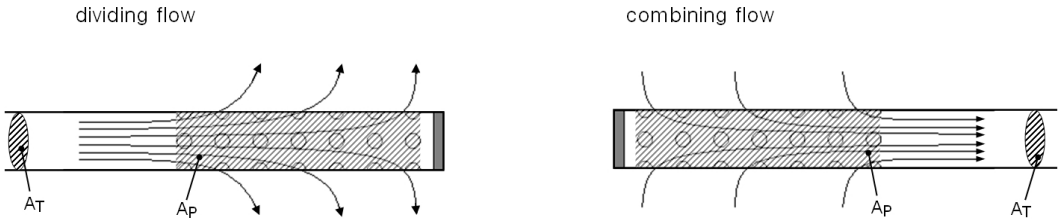

Figure 12 – Distinction between dividing flow and combining flow

area of the pipe A_T. The effective discharge coefficient C_D is different from the discharge coefficient C_d with a correction factor as described in reference [32].

In figure 13 different values for the effective discharge coefficient are obtained for two examples, where Duct A(x) has a hole diameter of $d_h = 3.5$ mm with $\sigma = 19.6$ % and Duct B(+) a hole diameter $d_h = 5$ mm and $\sigma = 13.6$ %.

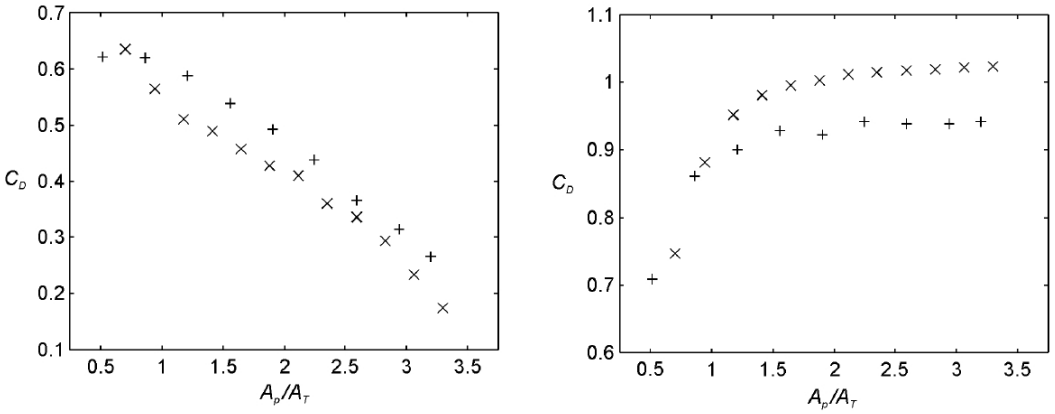

Figure 13 – Equivalent discharge coefficient in dividing flow (left) and combining flow (right): Duct A(x), Duct B(+) (cf. [32])

2.4 Higher order modes

When the dimensions of the muffler exceed a certain value and the wavelength is below a certain level, plane wave propagation can no longer be assumed (cf. figure 14) and higher order modes can be excited. Two kinds of modes can be distinguished namely *circumferential modes* m and *radial modes* n. At figure 15 those higher order modes are shown for circular ducts up to m=3, n=3. The dotted lines are *nodal lines* for transverse pressure distribution in the duct. Below every individual illustration of a mode the Helmholtz number ka is specified, where k is the wavenumber and a the radius of the chamber.

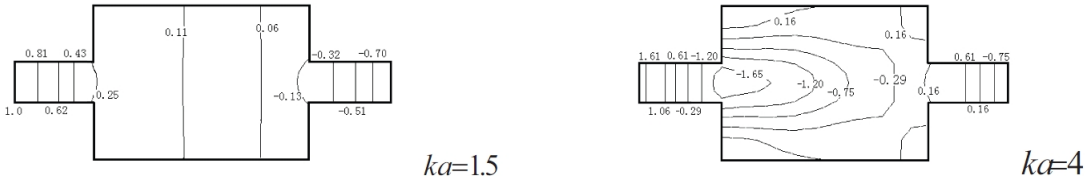

Figure 14 – Acoustic pressure contours in a muffler from reference [33]

At very low frequencies only the m=0, n=0 or plane wave mode can propagate so the pressure distribution is uniform across the duct as seen in figure 14 (left). Each higher order mode has a particular cut-off frequency below which it is not possible for that mode to propagate [34]. In concentric expansion chambers usually the first higher order mode is not excited but nevertheless plane wave propagation in general is just valid up to the cut-off frequency of the first circumferential mode (m=1, n=0):

$$f_c = \frac{1{,}84c}{\pi D} \tag{2.8}$$

where c is the speed of sound and D is the diameter of the chamber. Furthermore for a concentric expansion chamber the first higher order mode usually excited is the first radial mode at m=0 and n=1 and a cut off frequency at:

$$f_c = \frac{3{,}83c}{\pi D} \tag{2.9}$$

In chapter 4 it can be observed that for axial symmetric mufflers the first circumferential mode is not exited but the first radial mode usually is. E.g. for the eccentric plug muffler

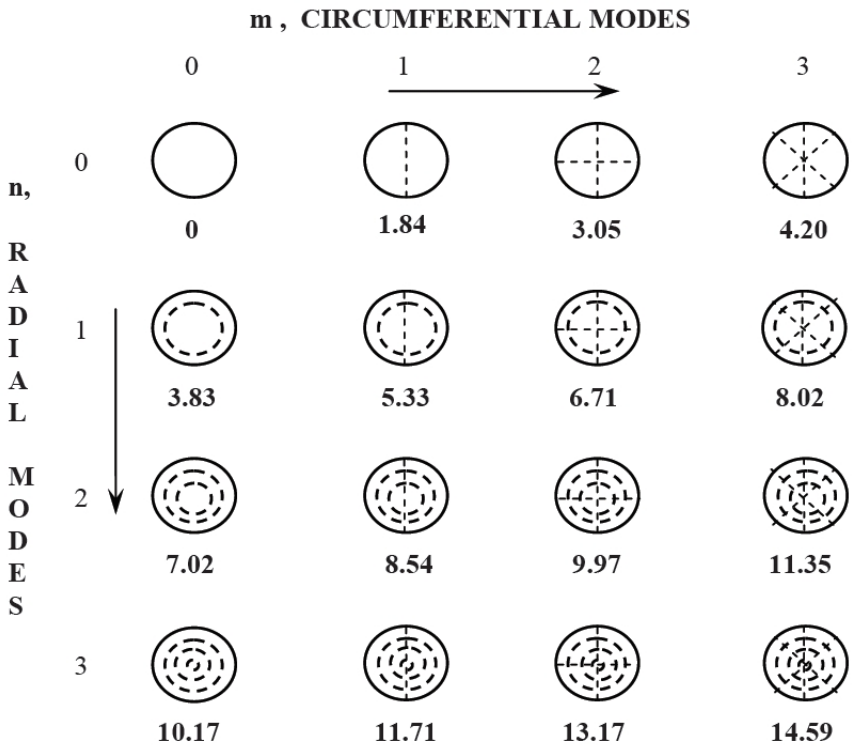

Figure 15 – Higher order modes [28]

the first circumferential mode is exited. More detailed observations concerning higher order mode effects and the influence of perforated pipes on them is discussed in the sub chapters for the particular muffler type.

2.5 Acoustic properties and measurement techniques

There are several acoustic properties to describe the damping behaviour of a muffler. Acoustic measurements can obtain results for *noise reduction*, *insertion loss* and *transmission Loss*. Noise reduction is the sound pressure level difference across the muffler. It is easy to measure but it is not exclusively dependent on the muffler. Insertion loss is the sound pressure level once determined with the muffler installed and once determined without the muffler. Therefore it provides realistic results under real conditions.

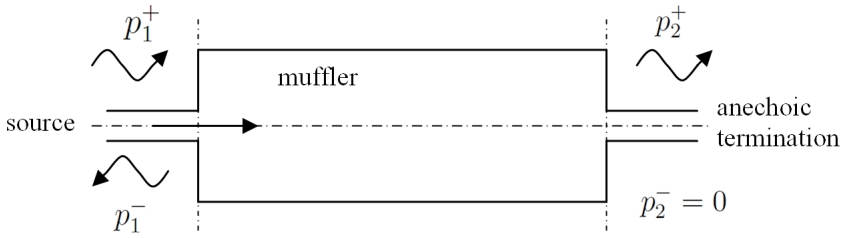

Figure 16 – Configuration for determination of transmission loss [35]

The transmission loss describes the sound power level difference between the incident and the transmitted wave. It requires an anechoic termination at the upstream end of the muffler as seen in figure 16. This idealistic assumption has the advantage that it describes the properties of the muffler itself, but the disadvantage that it is difficult to accomplish a fully anechoic termination. The transmission loss can be written as follows [35][4]:

$$TL = 20\,log\left(\frac{p_1^+}{p_2^+}\right)_{p_2^-=0} [dB], \tag{2.10}$$

where p_1^+ is the incident sound pressure and p_2^+ the transmitted sound pressure. Measurements of the transmission loss can be accomplished using the *decomposition method*, the *two load method*, or the *two source method*. The description of the following overview is mainly referred from Tao and Seyberts [36].

Decomposition method

The decomposition method obtains the transmitted sound pressure directly and the incident sound pressure by decomposition due to calculation of the auto spectra and cross

spectra between the two microphones at the upstream end. To apply the decomposition method an anechoic termination is required. This is achieved by using a long exhaust tube, high absorbing materials, horn shaped pipes or an active sound anechoic termination. The problem is that a fully anechoic termination is still difficult to build especially for low frequencies.

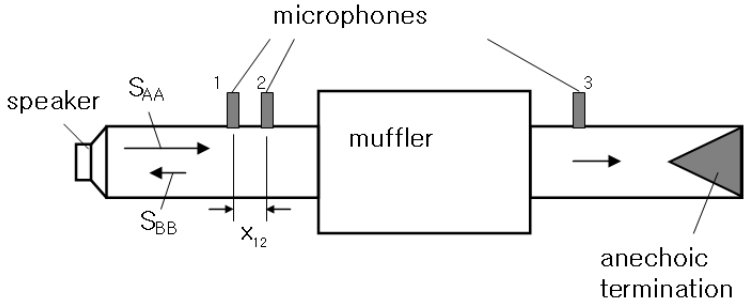

Figure 17 – Setup of decomposition theory

As seen in equation 2.10 the incident sound pressure and the transmitted sound pressure is required to calculate the transmission loss. The transmitted sound pressure can be measured directly at the outlet at point 3. To obtain the incident sound pressure the total sound pressure can be decomposed into its incident and reflected spectra S_{AA} and S_{BB} respectively. The incident sound pressure p_1^+ can be obtained by calculating the auto spectrum S_{AA} as follows:

$$p_1^+ = \sqrt{S_{AA}} = \sqrt{\frac{S_{11} + S_{22} - 2C_{12}\cos kx_{12} + 2Q_{12}\sin kx_{12}}{4\sin^2 kx_{12}}}, \tag{2.11}$$

where S_{11} and S_{22} are the auto spectra of the total acoustic pressure at point 1 and 2, respectively. C_{12} and Q_{12} are the real and imaginary parts of cross spectrum between points 1 and 2, k is the wave number and x_{12} is the distance between the two microphones (cf. [36]).

Two source method and two load method

To get two different configurations for solving the set of equations which is briefly described below the source can be switched as for the two source method (figure 18) or the load can

be changed as for the two load method (figure 19). The two load method is often easier to accomplish because the source does not have to be moved. Often this is achieved by one tube with absorbing material and the other tube without. If the two loads are too similar the result will be unstable. For the two load method the two loads have to be assumed different enough to achieve an accurate result, than the two source method might be the better choice. To obtain two different sources it is also possible to reverse the muffler.

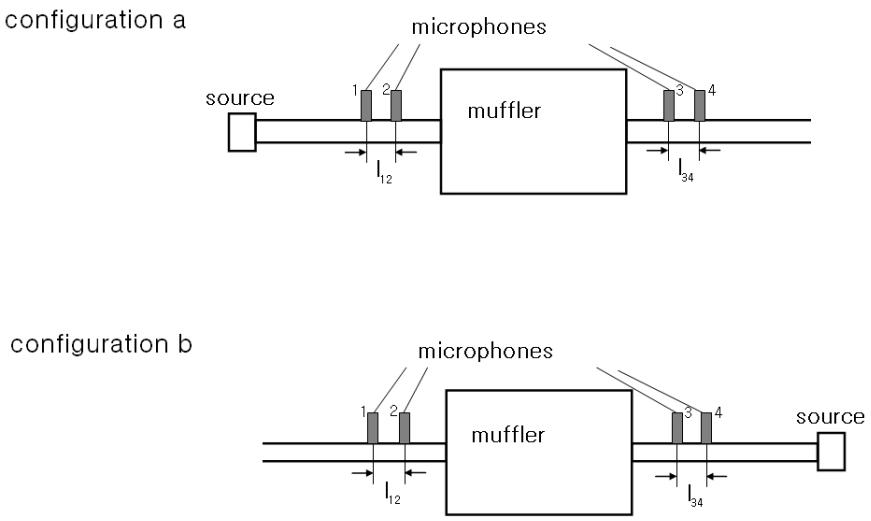

Figure 18 – Setup of two source method

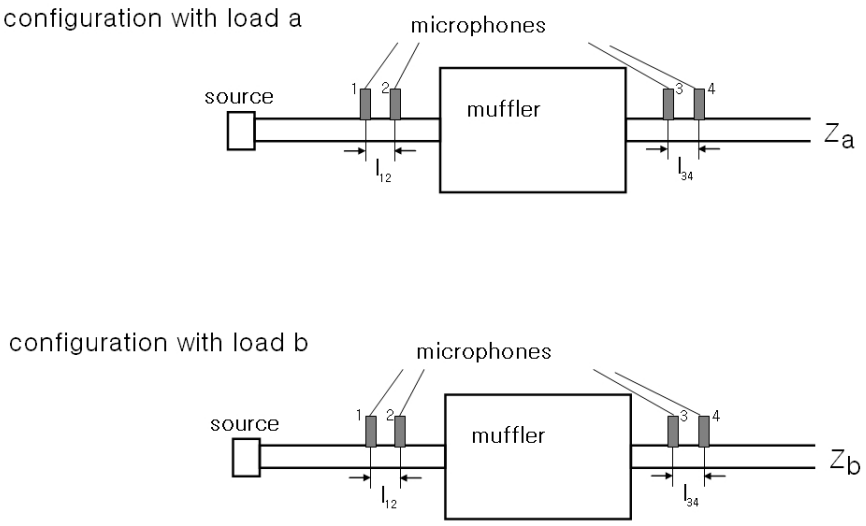

Figure 19 – Setup of two load method

Transfer matrix approach Both the *two source method* and the *two load method* are based on the transfer matrix approach. Therefore, the four pole parameters between measuring points 2 and 3 as seen in figure 18 and 19 are used to calculate the transmission loss. Figure 20 shows the general acoustical element. The corresponding transfer matrix is:

$$\begin{bmatrix} p_1 \\ v_1 \end{bmatrix} = \begin{bmatrix} A & B \\ C & D \end{bmatrix} \begin{bmatrix} p_2 \\ v_2 \end{bmatrix} \tag{2.12}$$

,

where p_1 and v_1 are sound pressure and particle velocity at the inlet and p_2 and v_2 at the outlet. A, B, C and D are the four pole parameters of the system.

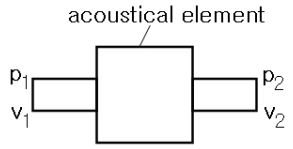

Figure 20 – The four poles

The four pole parameters between measuring points 2 and 3 are required to obtain the transmission loss which is:

$$TL = 20 \cdot \log \left[\frac{1}{2} \left| A_{23} + \frac{B_{23}}{\rho c} + \rho c \cdot C_{23} + D_{23} \right| \right] \ , \tag{2.13}$$

under the assumption that the cross section area does not change between inlet and outlet pipe. To obtain the four pole parameters A_{23}, B_{23}, C_{23} and D_{23} the pressure at all four measuring points for two configurations a and b (see figure 18) are measured and used in a set of equations which contains the transfer matrices between measuring points 1-2, 2-3 and 3-4. The following two transfer matrices describe the straight tube elements assuming that mean flow can be neglected:

$$\begin{bmatrix} A_{12} & B_{12} \\ C_{12} & D_{12} \end{bmatrix} = \begin{bmatrix} \cos kl_{12} & j\rho c \sin kl_{12} \\ j \sin kl_{12}/(\rho c) & \cos kl_{12} \end{bmatrix}, \qquad \Delta_{12} = 1 \tag{2.14}$$

$$\begin{bmatrix} A_{34} & B_{34} \\ C_{34} & D_{34} \end{bmatrix} = \begin{bmatrix} \cos kl_{34} & j\rho c \sin kl_{34} \\ j \sin kl_{34}/(\rho c) & \cos kl_{34} \end{bmatrix}, \qquad \Delta_{34} = 1 \ , \tag{2.15}$$

where l_{12} and l_{34} are the spacing between points 1-2 and 3-4. With the measured data and the transfer-matrices equations (2.14) and (2.15) the four pole parameters for the unknown system between points 2 and 3 are solved as follows:

$$A_{23} = \frac{\Delta_{34}(H_{32a}H_{34a} - H_{32b}H_{34a}) + D_{34}(H_{32b} - H_{32a})}{\Delta_{34}(H_{34b} - H_{34a})} \tag{2.16}$$

$$B_{23} = \frac{B_{34}(H_{32a} - H_{32b})}{\Delta_{34}(H_{34b} - H_{34a})} \tag{2.17}$$

$$C_{23} = \frac{(H_{31a} - A_{12}H_{32a})(\Delta_{34}H_{34b} - D_{34}) - (H_{31b} - A_{12}H_{32b})(\Delta_{34}H_{34a} - D_{34})}{B_{12}\Delta_{34}(H_{34b} - H_{34a})} \tag{2.18}$$

$$D_{23} = \frac{B_{34}(H_{31a} - H_{31b}) - A_{12}(H_{32b} - H_{32a})}{B_{12}\Delta_{34}(H_{34b} - H34a)} \ , \tag{2.19}$$

where $H_{ij} = p_j/p_i$, which are measured with i and j are the measuring points 1-4. Δ_{34} is the determinant of the transfer matrix between point 3 and 4.

3 Equations and implementation

In this chapter the numerical method used for the 3D cell approach is described and further this method is extended with the implementation of the perforated connector. Because of the advantages of the Finite volume method the simulation tool AVL Boost is based on it. The modelling of perforations is based on the method proposed by G. Montenegro et al. [23], which is the only available published solution at present. Two parameters namely the friction factor f and the end correction coefficient α are taken into account of the perforated connector. These are considered in the second subchapter.

The most complete mathematical description of the flow of fluids are the Navier Stokes equations in three dimensions. They are very difficult to solve and it is possible to obtain an analytical solution only for very simple geometries, so their practical relevance is limited. Because internal stresses can be neglected - when the flow is far from solid surfaces - this leads to the simplified *Euler-equations* for inviscid fluids. These are commonly used to study compressible flows at high Mach numbers. The fact that no boundary layer near the walls need be resolved allows the use of coarser grids (cf. [16]). Because of high Mach numbers also high Reynolds numbers occur which means the flow is said to be turbulent or unsteady flow (see figure 21) where $u(t) = u + u'$.

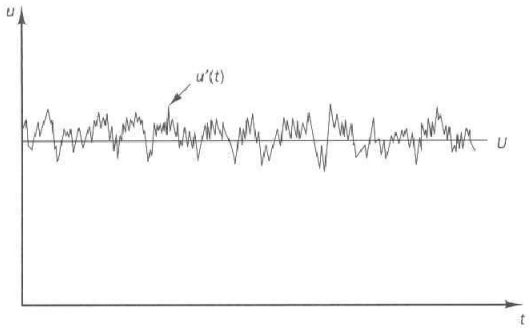

Figure 21 – Typical point velocity measurement in turbulent flow (cf.[37])

The described three-dimensional model is a staggered grid approach and it can be coupled with one-dimensional models which is common practice as the flow through the pipes, which connect the engine with the exhaust muffler, can be considered to be one-dimensional. This is also applied for the simulations done in chapter 4.

From 1D to 3D A fluid dynamic model must solve the spatial and temporal variations of the flow. For this the set of hyperbolic differential equations (3.1), (3.2) and (3.3) are solved by one dimensional non linear continuity, momentum, and energy equations. To take into account the resistance which appears when the flow passes the walls of the pipes a wall friction and heat transfer between the gas and the pipe walls is considered in the formulation of the models cf.[17].

One-dimensional CFD-codes are already well established but since the plane wave approach does not take into account the higher order modes the accuracy of these models is limited. Another disadvantage is that prior knowledge of the acoustic behaviour of muffler sections are necessary to model them correctly. With the generic 3D acoustic cell element introduced in [4] it is possible to predict the acoustic behaviour of the muffler based on its geometry only. Therefore a mesh of 3D cells based on the geometry of the muffler is created.

3.1 Finite volume method

In general on the theory of the Finite Volume Method one can say that the solution domain is subdivided into a finite number of contiguous control volumes by a grid which, in contrast to the finite difference method, defines the control volume boundaries, not the computational nodes cf.[16]. Control volumes are defined by a suitable grid where the computational node is usually in the centre of the control volume. As seen in Figure 22 it is also possible that the boundary is on half way between two computational nodes. However the first variant is used more often and is solely referred in this work.

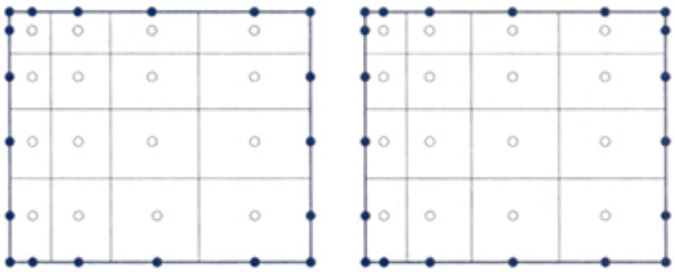

Figure 22 – Types of Finite Volume grids: nodes centred in control volume (left) and control volume faces centred between nodes (right)[16]

In figure 23 typical *staggered grid control volumes* are shown:

The control volume for the solution of mass- and energy equation and other scalar quantities is displayed on the left. The control volume for solving the momentum equation in x and y direction for two dimensionality is displayed in the centre and right.

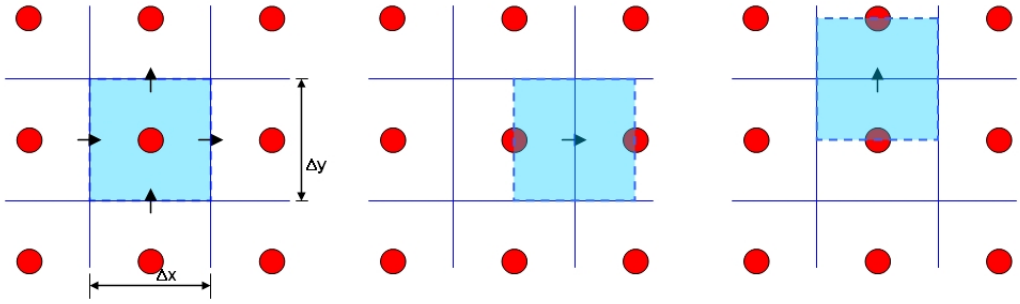

Figure 23 – Control volumes for a staggered grid: for mass conservation and scalar quantities (left), for x-momentum (center) and for y-momentum (right) (cf. [16])

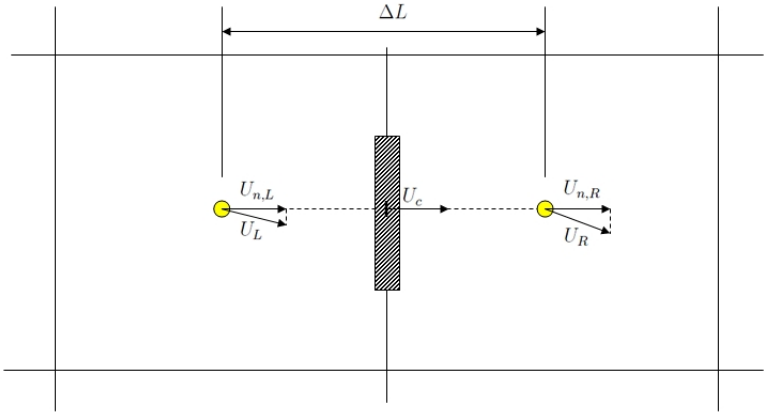

Figure 24 – Model of two 3D cells with connector

Every 3D cell has a certain volume and is connected to the neighbouring cell with a connector also often called a port. In figure 24 the linkage between two 3D cells due to one connector is illustrated, but the actual shape of a 3D cell is arbitrary. Just for better illustration its rectangular. For the linkage between two adjacent 3D cells the normalized velocity vectors $U_{n,L}$ and $U_{n,R}$ are needed as seen in figure 24. The subscript n, which here stands for "normalized" is left out in all following formulas not to confound it with

the time step superscript .

The total volume of the muffler is generated as a mesh of 3D cells with a reasonable accuracy for the correct acoustic prediction. As mentioned before the solution of this mesh of 3D cells is based on a staggered grid approach where the control volumes either are defined over a volume or a connector, but the 3D cells themselves are spatially fixed. The equations of mass and energy are solved at cell centres and the momentum equation at cell connections or boundaries [4] [37]. Because the viscosity of the gas in the system is very low it can be neglected and therefore the mathematic equations for unsteady flow in a compressible fluid will lead to the Euler formulation for the Navier-Stokes equations. Therefore the equations for continuity (mass conservation), momentum and energy in coordinate-free form can be given as follows [17]:

$$\frac{\partial \rho}{\partial t} + div(\rho \mathbf{U}) = 0, \tag{3.1}$$

$$\frac{\partial (\rho \mathbf{U})}{\partial t} + div(\rho \mathbf{U} \times \mathbf{U}) = -divp, \tag{3.2}$$

$$\frac{\partial (\rho E)}{\partial t} + div(\rho E \mathbf{U}) + div(p\mathbf{U}) = 0, \tag{3.3}$$

where ρ stands for density, t for time, $\mathbf{U}$ for the fluid velocity and E for the specific stagnation internal energy. Equation (3.1) expressed in Cartesian coordinates leads to:

$$\frac{\partial \rho}{\partial t} + \frac{\partial (\rho \mathbf{U}_i)}{\partial x_i} = \frac{\partial \rho}{\partial t} + \frac{\partial (\rho U_x)}{\partial x} + \frac{\partial (\rho U_y)}{\partial y} + \frac{\partial (\rho U_z)}{\partial z} = 0, \tag{3.4}$$

where x_i $(i = 1, 2, 3)$ or (x, y, z) are the Cartesian coordinates and $\mathbf{U}_i$ or (U_x, U_y, U_z) are the Cartesian components of the velocity vector $\mathbf{U}$ [16]. Equations (3.2) and (3.3) can be handled in the same way. The continuity and energy equation integrated in time over the volume leads to the following discretized form:

$$\rho^{n+1} = \rho^n + \frac{1}{V} \sum_{c=1}^{N_c} \left(\rho_c^n U_c^n A_c^n \right) \Delta t \tag{3.5}$$

$$(\rho E)^{n+1} = (\rho E)^n + \frac{1}{V}\Big(\sum_{c=1}^{N_c} \rho_c^n E_c^n U_c^n A_c^n + \sum_{c=1}^{N_c} p_c^n U_c^n A_c^n\Big)\Delta t, \tag{3.6}$$

where the subscript c indicates the connector and N_c is the total number of connectors linked to the cell [4]. The superscripts n and $n+1$ indicate the actual and next calculation time step. U_c is the gas velocity at the connector oriented in a direction normal to the connector (see Figure 24). A_c is the connectors surface area. Both equations are solved at the cell centres out of the summation of the values at the connectors - see figure 23 left, where the arrows indicate the incident or leaving intensive property. Different to cell centre calculation the momentum and velocity are calculated at the connectors as follows (see also figure 23 (center) (right)). Taking into account the balance between the pressure force and momentum of the neighbouring cells, namely left and right cells the momentum equation is solved as follows [4] [38]:

$$\dot{m}_c^{n+1} = \dot{m}_c^n + \left[\left(\dot{m}_c^n U_L^n - \dot{m}_c^n U_R^n\right) + \left(p_L^n - p_R^n\right) A_c\right] \frac{\Delta t}{\Delta L}, \tag{3.7}$$

where $\dot{m} = \rho U A$ is the mass flux through the connector and ΔL is the length between two adjacent 3D cells. Once the momentum at the connector is calculated, the cell momentum can be determined by summation of the momentum fractions of all connectors:

$$(\rho U V)_{Cell} = \sum_{c=1}^{N_c} (\rho U A)_c \, \Delta L_c, \tag{3.8}$$

where ΔL_c is the distance between cell centre and the connector. To obtain the momentum fraction according to the actual cell the massflow at every connector is multiplied with the corresponding distance ΔL_c.

Solution of the governing equation The three equations for mass conservation, energy conservation and the momentum equation contain four unknowns ρ, U, p and E. To solve the problem the *ideal gas* state equations are usually sufficiently accurate:

$$\frac{p}{\rho} = RT \qquad and \qquad E = c_v T, \tag{3.9}$$

where R is the specific gas constant, T the gas temperature and c_v the specific heat capacity at constant volume.

3.2 Implementation of the perforated connector

Also for the perforated connector the Euler formulation for the Navier Stokes equations comes into account (equations 3.1, 3.2 and 3.3). Different is, that the wall friction factor is introduced with a higher value compared to straight pipes, because it takes into account the additional friction caused by the gas stream on the edges of the holes. Also an appropriate mass end correction has to be considered.

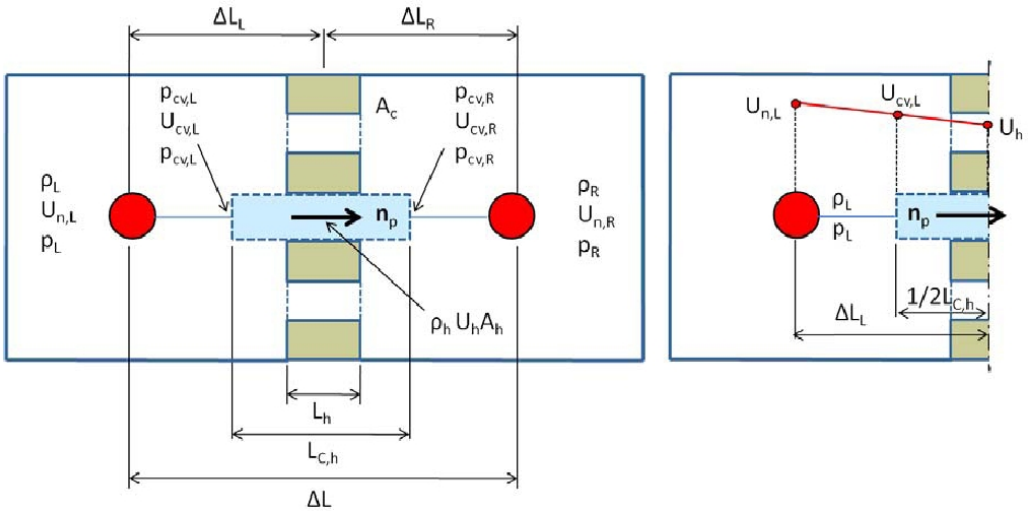

Figure 25 – Schematic of the perforated connector element [23]

The principle of the following description is mostly based on reference [23] so it is merely referred if literally cited. For the perforated connector a control volume, which is valid for a single hole of the perforation, is defined. Therefore it takes into account its diameter d_h, its wall thickness L_h and the end correction length Δl so that the corrected wall thickness is:

$$L_{C,h} = L_h + 2\Delta l \tag{3.10}$$

Under the condition that the wall thickness and the hole diameter are much smaller than the wavelength a hole will behave as a piston of air. The enclosed volume, built by the

hole diameter and the wall thickness, will push the air around both sides of a hole acting as an extra mass attachment. This extra attachment is called mass end correction as seen in figure 25 regarding to the fractions which are jutting out of the wall [39].
The end correction length is dependent on the hole diameter and independent of the wall thickness. In its most fundamental form, first introduced by Rayleigh [40] it is written as:

$$2\Delta l = 0.85 d_h \tag{3.11}$$

The value 0.85 is the end correction coefficient α, which was also mentioned in chapter 2.3 where Sullivan and Crocker [5] proposed $\alpha = 0.75$. Ingard [41] established a more accurate equation which takes into account the porosity σ:

$$\alpha = 0.8(1 - 1.4\sqrt{\sigma}) \tag{3.12}$$

Rschevkin [42] and later Müller [43] proposed an equation which is also valid for porosity levels greater than 20 %:

$$\alpha = 0.8(1 - 1.47\sqrt{\sigma} + 0.47\sqrt{\sigma^3}) \tag{3.13}$$

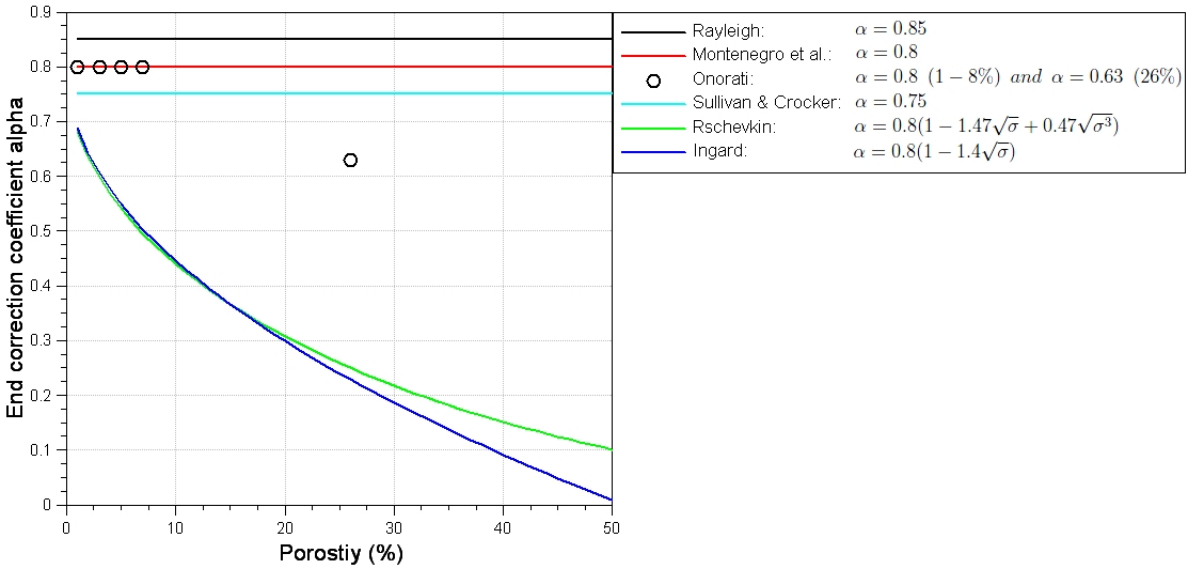

Figure 26 – End correction coefficient α in relation to the porosity

Onorati found $\alpha = 0.63$ appropriate for perforates with high porosity, where he just referred to 26 % porosity level, and $\alpha = 0.8$ for low porosities from 1-8 % (cf. [21] [18]). All simulations in chapter 4 are done with $\alpha = 0.8$ except for one example in chapter 4.2.1 for the single plug muffler where the behaviour of varying end correction length is investigated. As seen in figure 27 where pressure loss results, through the double plug muffler from chapter 4.2.2, show that no improvement of implementing equation 3.13 can be made. The friction factor was set to $f = 0.2$. The results accomplished with Rayleigh correction length fit the 28 % case, but for 14 % and 7 % they show overestimated pressure loss results. The results accomplished with Rschevkins correction length underestimate the pressure loss for 28 % and 14 %, but overestimate the 7 % case. It might be assumed that the resolution of the 3D cell meshes is too coarse so that the influence cannot be investigated properly, or that further experiments are necessary to investigate the relation between correction length, friction factor and porosity level.

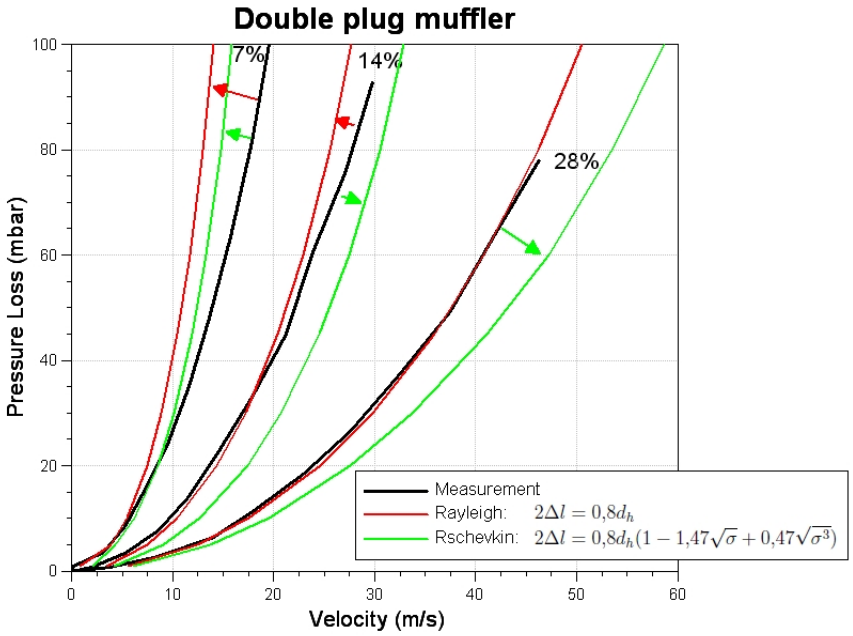

Figure 27 – Pressure loss with different correction lengths

The momentum equation (3.7) adopted for the single hole control volume, where $\dot{m}_h = \rho_h U_h A_h$ is the mass flow through a single hole, becomes as follows:

$$\dot{m}_h^{n+1} = \dot{m}_h^n + \left(\rho_L U_{CV,L}^2 - \rho_R U_{CV,R}^2 + p_L - p_R\right) A_h \frac{\Delta t}{L_{C,h}} - F_h \Delta t \tag{3.14}$$

To obtain the whole mass flow through the connector the mass flow through one single hole is multiplied by the number of holes through that connector. The velocities at the left and right boundary of the control volume $U_{CV,L}$ and $U_{CV,R}$ are interpolated values (cf. figure 25 (right)) and calculated as:

$$U_{CV,L} = \frac{\frac{1}{2}L_{C,h}U_{n,L} + \left(\Delta L_L - \frac{1}{2}L_{C,h}\right)U_h}{\Delta L_L}, \quad U_{CV,R} = \frac{\frac{1}{2}L_{C,h}U_{n,R} + \left(\Delta L_R - \frac{1}{2}L_{C,h}\right)U_h}{\Delta L_R} \tag{3.15}$$

The shear stress τ_W as seen in figure 28 can be expressed as [17]:

$$\tau_W = \frac{1}{2}\rho U^2 f \tag{3.16}$$

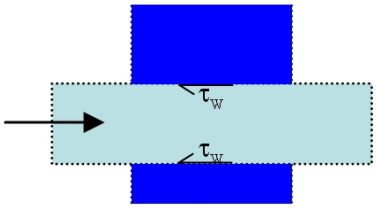

Figure 28 – shear stress on the control volume

Equation 3.16 enables the surface force on the control volume to be represented as [17]

$$-\frac{1}{2}\rho U^2 f \pi d_h dx \tag{3.17}$$

Further the term F_h in the momentum equation 3.14 where f is the friction factor is determined as follows [17]:

$$F_h = \tau_W d_h \pi = (\rho U A)_h |U_h| f \frac{2}{d_h} \tag{3.18}$$

In chapter 4 the friction factor f is varied and its influence on the acoustic and performance results (pressure loss) is observed. Also the influence of the end correction coefficient α on the acoustic results is investigated.

4 Investigations of different muffler types

In this chapter several basic muffler types are investigated and simulation results are compared to measurement results. For all muffler types comparisons of the transmission loss are made. For the single, double and eccentric plug muffler also pressure loss simulations are compared to measurements. Several factors which are influencing the accuracy of the solution are investigated:

- 3D cell mesh accuracy
- Spatial pipe discretization at the inlet and outlet pipe
- Friction factor f
- End correction coefficient α
- Number of cycles

The non linear solver in Boost comprises a full engine simulation. One revolution of the crankshaft is referred as one cycle. For all simulations the reference speed is set to 1200 rpm for a 4 Stroke engine.

For simple muffler types, like those presented in this chapter, at least 7 simulation cycles are recommended to obtain accurate simulation results, therefore commonly 10 - 15 simulation cycles are used. Simulations with mean flow usually require some more cycles than simulations without mean flow. For most of the test cases three different mesh accuracies are tested with 3D cell side length of approximately 20 mm, 30 mm and 40 mm. Simulation results with the 30 mm mesh give the best congruence with measured data for all tested muffler types therefore if not explicitly mentioned all simulations are done with the 30 mm mesh.

The simulations of pressure loss are accomplished with 3 cycles. The inlet pressure is increased stepwise to obtain the associated velocity in order to get the characteristic curve. For all pressure loss simulations the results are not influenced by the mesh accuracy or the spatial pipe discretization.

Mesh generation

For the mesh generation the volume of the exhaust chamber has to be modelled out of a certain amount of 3D cells. The 3D cell side length is an input parameter for the mesh generation. In order to model the mufflers volume, diameter and total length correctly the 3D cell side length is automatically varied a little bit. For example, if the input mesh size is 30 mm and the length of the muffler is 256 mm, it will be modelled out of 8 cells with a cell side length of 32 mm.

Unfortunately the meshing of the perforated pipe in Boost, at the present stage of the development, is limited to one dimensionality, which means that the 3D cells are all ordered in one straight line. It might be assumed that the accuracy for simulation results, especially for non-concentric positioning of the perforated pipes in the exhaust chamber, is limited.

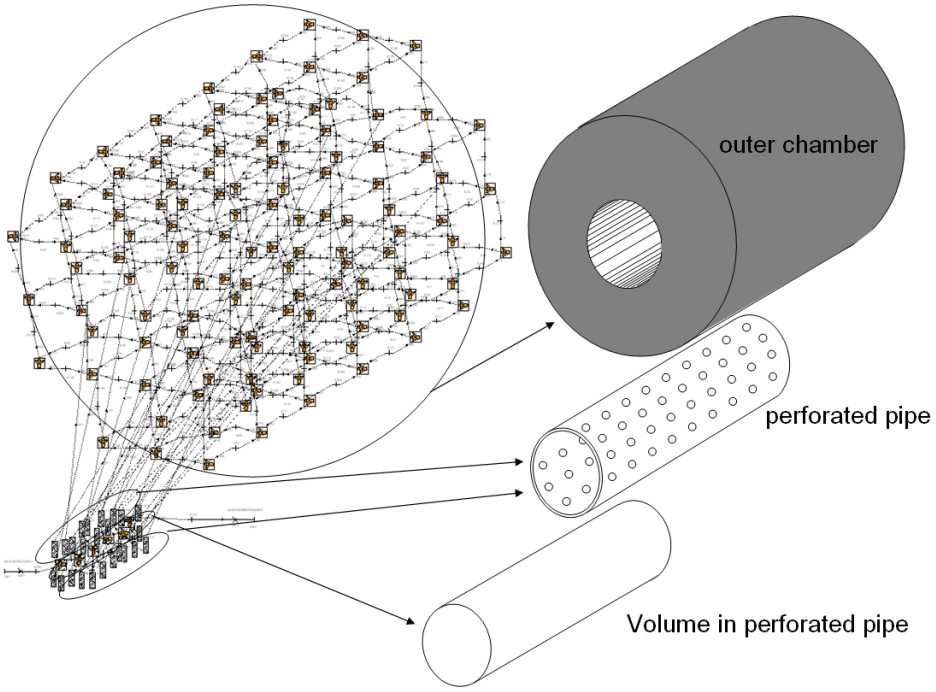

Figure 29 – 3D cell mesh for a simple through flow muffler

As seen in figure 29 the Volume is modelled as a mesh out of a certain amount of 3D cells. The mesh in the upper part presents the outer chamber of the muffler, the set of 3D cells in the lower part presents the volume inside the perforate pipe. To model the perforated pipe the cells inside the pipe are connected with the chamber cells due to four perforated

connectors in every perpendicular direction which is pictured in figure 30.

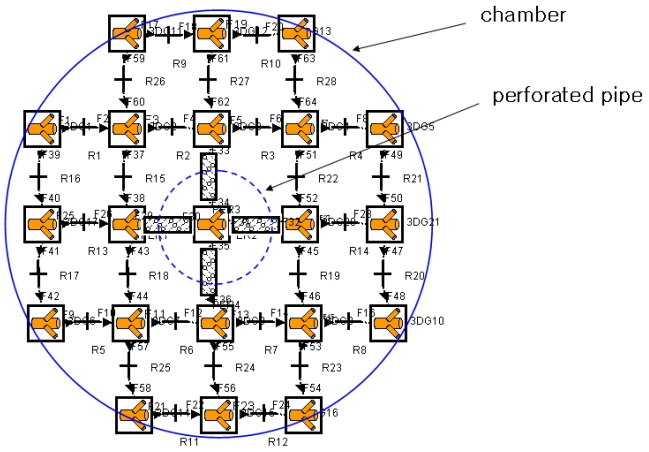

Figure 30 – Scheme of a mufflers cross-section

System boundaries

For the simulation the system boundaries are modelled as an acoustic source at the inlet pipe (SB1) and anechoic termination at the outlet pipe (SB2) of the muffler to set the conditions for determination of the transmission loss as illustrated in figure 31.
The acoustic source is set to white noise perturbation with $\Delta p = 0.5$ mbar. With a reference pressure level of $p_0 = 20\ \mu$ Pa for air, according to equation 4.1, this leads to a sound pressure level of $L = 128$ dB.

$$L = 20\,log\left(\frac{p}{p_0}\right)[dB] \tag{4.1}$$

For simulations without mean flow the mean pressure at the system boundaries are both set to 1 bar. For simulations with mean flow the mean pressure at the inlet system boundary is set to a higher value than the outlet system boundary to achieve the desired Mach number (e.g. M=0.05 or M=0.1).

The inlet and outlet pipes which connect the system boundaries with the 3D cell mesh are modelled as straight pipes which use the one-dimensional ENO finite volume scheme. Those have as an input parameter the spatial pipe discretization which can be seen in figure 32. For most of the tested muffler types it is set to 5 mm or 10 mm.

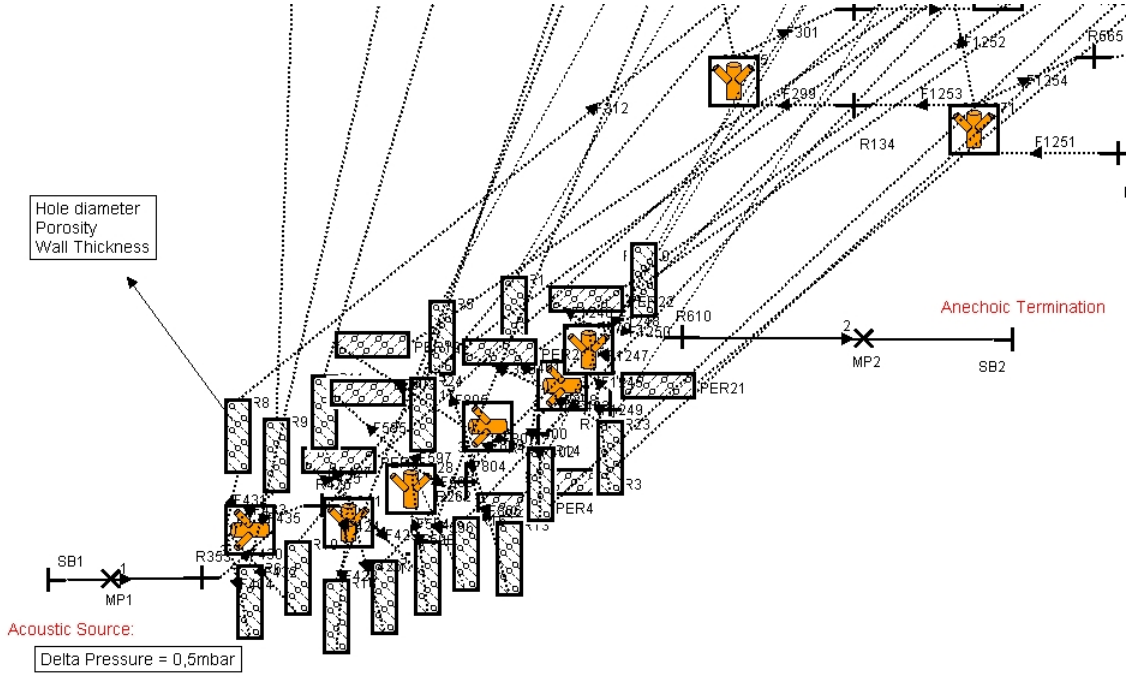

Figure 31 – System boundaries set as acoustic source and anechoic termination for transmission loss simulation

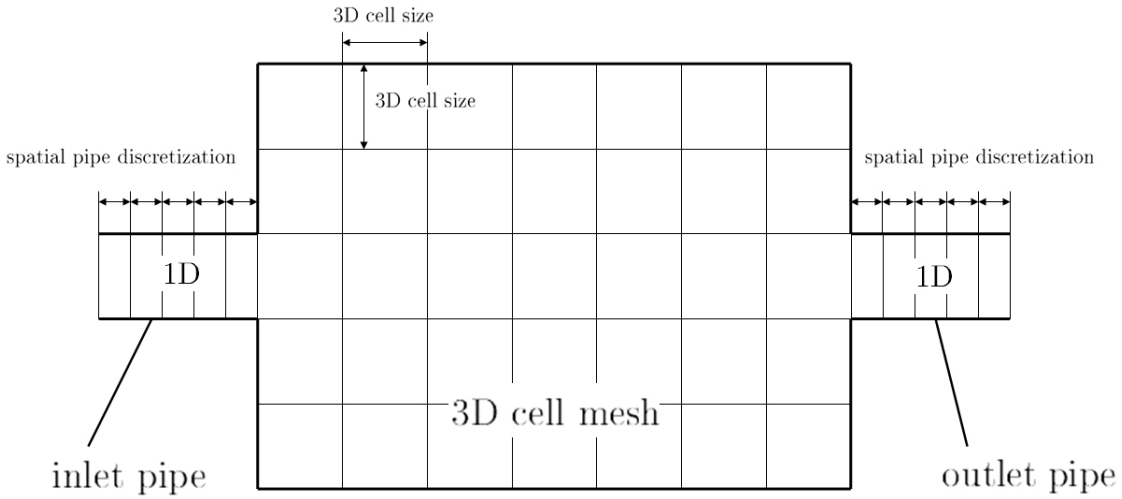

Figure 32 – 3D cell size vs. spatial pipe discretization

4.1 Through flow mufflers

A through flow muffler consists of an empty expansion chamber where a perforated pipe is connected to the inlet and outlet pipe (see figure 33 and 43). Two mufflers of different size and volume are investigated. Simulations of the transmission loss are done and results are evaluated and compared to measurements. All results are without mean flow.

4.1.1 Through flow muffler - short chamber

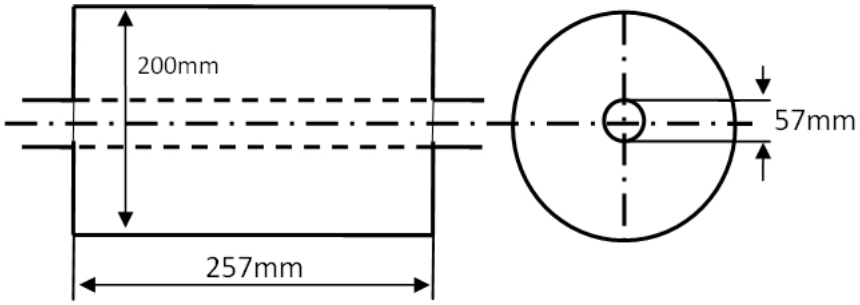

Figure 33 – Scheme: Through flow muffler - short chamber

The chamber and the perforated pipe have a total length of 257 mm, the diameter of the chamber is 200 mm, the perforated pipe diameter and the inlet pipe and outlet pipe diameter is 57 mm. Simulations are done with different mesh sizes and friction factors. As seen in figure 29 the Volume is modelled as a mesh out of a certain amount of 3D cells. The approximate side lengths of the models with 126, 297 and 1001 3D cells are 40, 30 and 20 mm, respectively. The physical volume of the muffler is about 8 litres which is modelled accurately by all the 3D cell meshes.

For the following results the geometry of the muffler remains the same, but the hole diameter and porosity level of the perforated pipe is varied according to table 1.

Pipe	d_h	Porosity	Thickness
1	3 mm	12 %	1.2 mm
2	4 mm	12 %	1.2 mm
3	5 mm	11 %	1.2 mm
4	8 mm	13 %	1.2 mm
5	5 mm	5.5 %	1.2 mm

Table 1 – Perforated pipes physical data

Influence of spatial pipe discretization: In figure 34 the influence of the spatial pipe discretization of the inlet and outlet pipe is shown. The best appropriate value for pipe cell discretization for this case is 5 mm. With increasing pipe cell discretization the overestimation is further increasing. For 10 cycle simulation the required computational time for 5 mm pipe discretization is the longest. All simulations in figure 34 are done with 10 cycles.

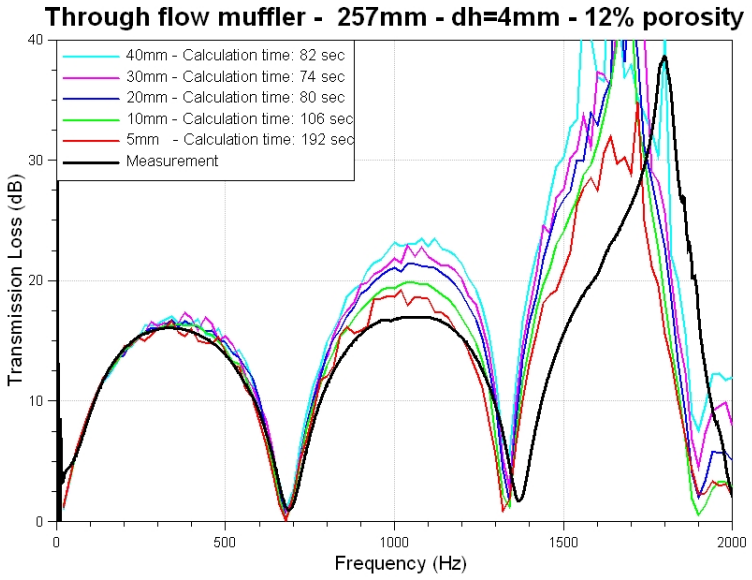

Figure 34 – Test case with pipe 2 - different spatial pipe discretization of the inlet and outlet pipe

Influence of mesh size: Simulation results with different mesh accuracies are shown in figure 35 and compared to measurement. It can be noted that the 30 mm mesh has less deviation concerning the frequency shift of the peak at around 1800 Hz than the 40 mm mesh. This frequency shift can also be observed at the second minima at around 1380 Hz and appears at all simulations. So it can be expected that the accuracy increases with finer meshes. Due to numerical miscalculations, which could not be investigated within the scope of this thesis, the 20 mm mesh gave worse results than the previous meshes.

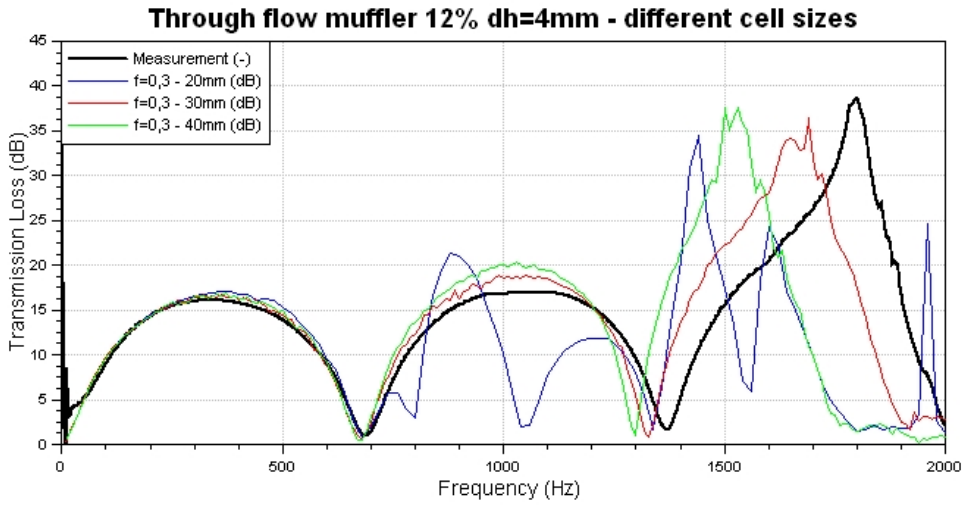

Figure 35 – Test case with pipe 2 - different mesh accuracies

Results and discussion

Figures 36 - 39 show transmission loss results with different perforated pipes according to table 1 with the 30 mm mesh. Results are compared to measurement and simulation results from the research report by Y. Guo [39]. Measurements where done at the Acoustic Competence Centre (ACC) in Graz which now is named Virtual Vehicle Competence Center (ViF). Simulations using the "Elnady model" [31], which uses a certain impedance model, where done by Y. Guo with Boost Linear Acoustic calculations.

It can be seen that the model is able to capture higher order mode effects. The first higher order mode would be at $ka = 1.84$, which gives a cut off frequency at approximately 1000 Hz. The product of k the wavenumber and a the radius of the chamber

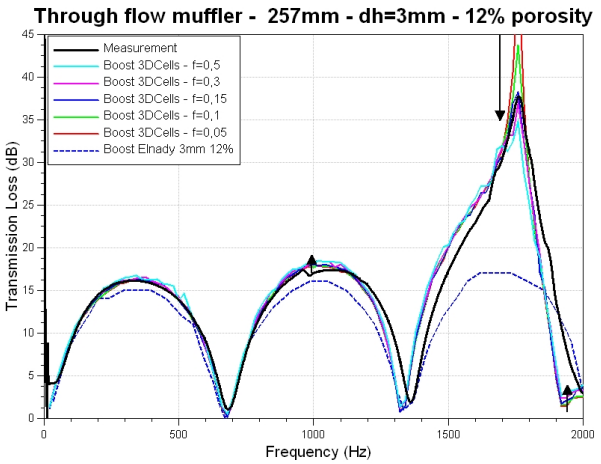

Figure 36 – Test case with Pipe 1

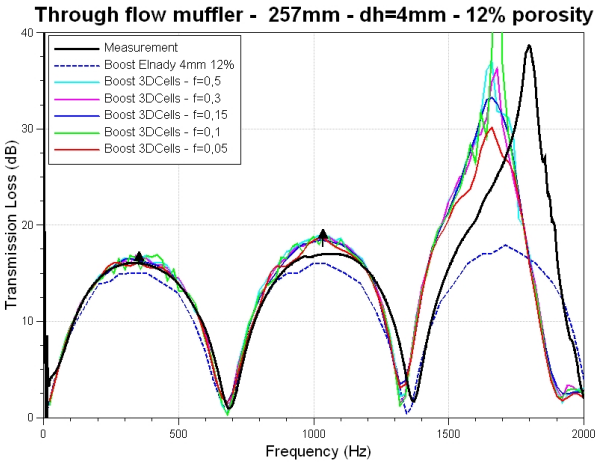

Figure 37 – Test case with Pipe 2

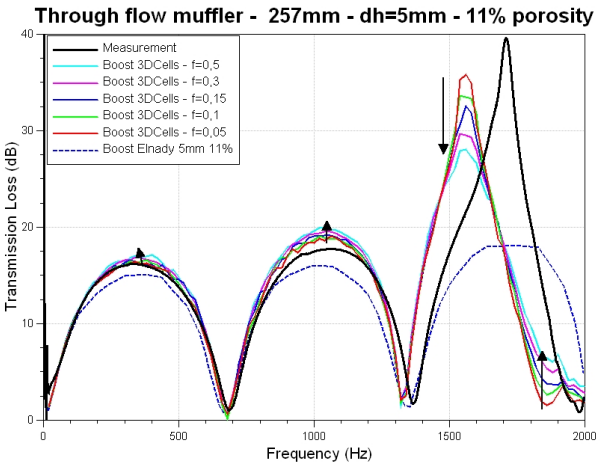

Figure 38 – Test case with Pipe 3

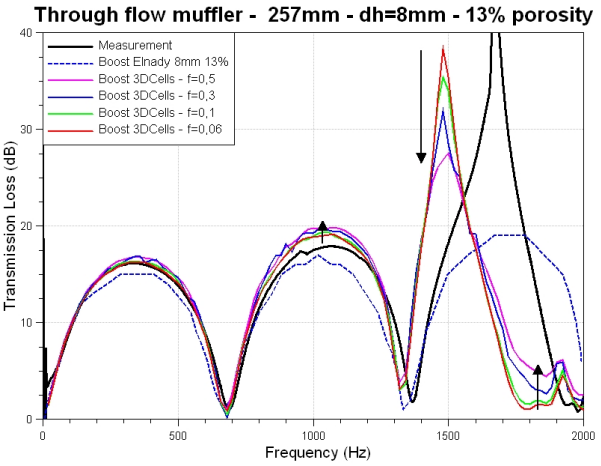

Figure 39 – Test case with pipe 4

is referred to as the Helmholtz number. As discussed in chapter 2.4 above the cut off frequency at $ka = 1.84$ the plane wave theory may be inadequate to describe the performance of the chamber (cf.[34]). For the present muffler type which is an axial symmetric configuration the first circumferential mode is not exited but the first radial mode at $ka = 3.83$ at around 2090 Hz is excited. Therefore the peak at around 1700 Hz is particularly increased. This can be observed at the simulation results done with Boost 3DCells. In contrast Boost Linear Acoustics with the impedance model by Elnady [31] can not capture the higher order mode effect.

At figure 40 the frequency range is extended to 3000 Hz. Simulations with different porosity levels are done with the same hole diameter. At a porosity level of 50 % the

behaviour is very similar to that of an empty expansion chamber and it can be assumed that, despite the already known frequency shift, the prediction is correct because typical for the acoustic behaviour the damping is decreased above the cut off frequency of the first radial mode (m=0, n=1). At 20 % porosity the peak at around 1800 Hz appears from the influence of the perforated pipe, which is an emprovement of the damping behaviour. This peak is shifted to lower frequencies with decreasing porosity level as the arrows in the figure indicate.

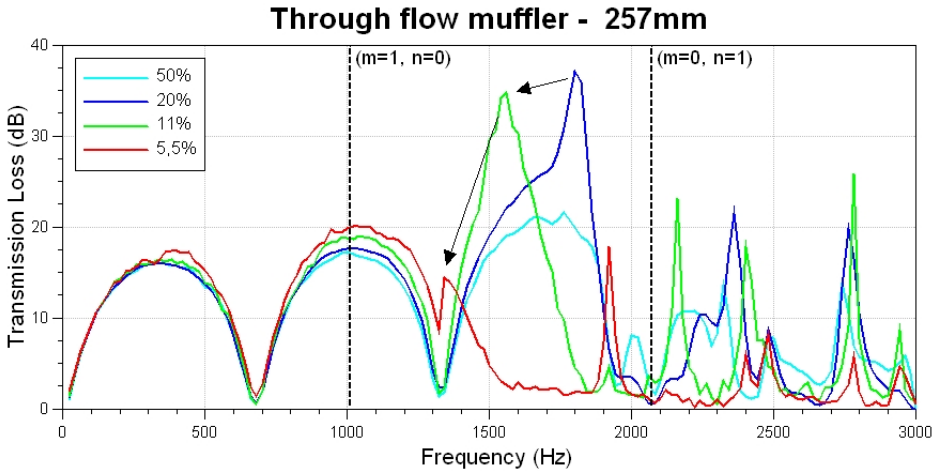

Figure 40 – Simulations with different porosity levels

Simulation results with different temperatures at figure 42 show how the whole characteristic curve shifts to higher frequencies when simulated with higher gas and wall temperature.

For all test cases the influence of the friction factor is as follows:

- In the frequency range from 0 - 700 Hz no significant difference..
- From 700 - 1300 Hz the transmission loss is increased with greater friction.
- The peak maximum is lower with high friction factor, that means peaks are smoothed with higher friction factors. This can be clearly see in figures 36, 38, 39 and 41, but results in figure 37 do not clearly show the same behaviour for the peak. This might be due to numerical instabilities.

For all simulation results a friction factor between $f = 0.05$ - 0.15 seems fit best to the measured transmission loss.

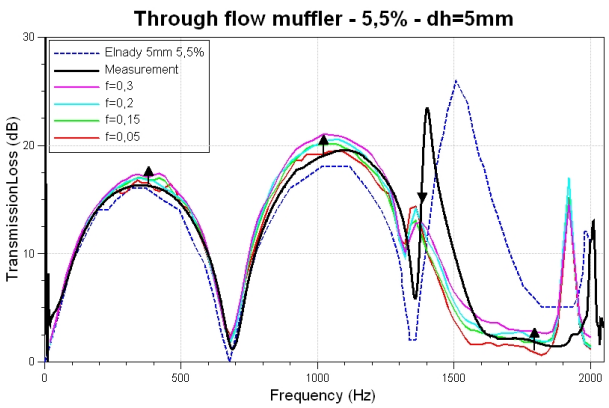

Figure 41 – Test case with Pipe 5

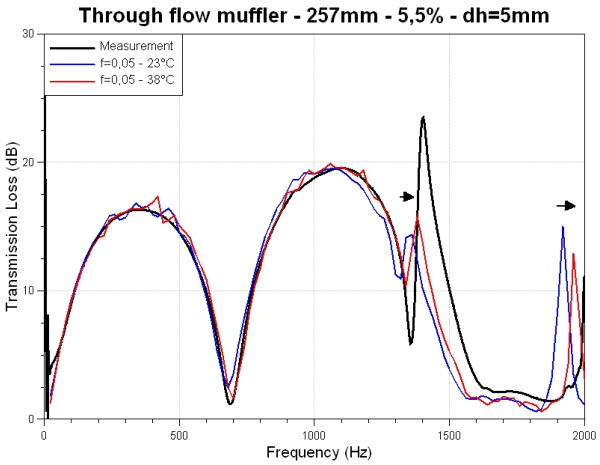

Figure 42 – Pipe 5: different temperatures

4.1.2 Through flow muffler - long chamber

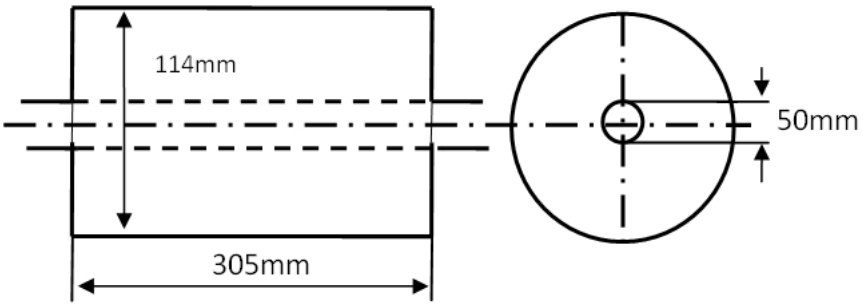

Figure 43 – Scheme: Through flow muffler - long chamber

To analyse the behaviour of the present muffler, which has a smaller diameter and a longer chamber length as the previous example (cf. figure 33), also simulation results of the transmission loss are compared to measurements. Different hole diameters and porosity levels of the perforated pipe, as listed in table 2, are investigated. To distinguish from the previous examples here the pipes are labelled with capital letters.

The measurements for the present muffler type where all taken from Morel et al.[44] conducted at room temperature. The measured transmission loss ranges up to 3000 Hz.

Influence of mesh size For the simulations three different cell sizes are tested. Cell sizes of approximately 20 mm, 30 mm and 40 mm yield to 428, 170 and 72 3D cells respec-

Pipe	d_h	Porosity	Thickness
A	6.3 mm	40 %	1.6 mm
B	4 mm	4.7 %	1.6 mm
C	3.2 mm	3 %	1.6 mm
D	2.4 mm	1.7 %	1.6 mm

Table 2 – Perforated pipes physical data

tively. Each mesh captures the volume and diameter of the muffler volume accurately. As seen in figure 44 all different meshes give good results up to 1100 Hz. Above that value the predicted maximums and minimums are shifted to lower frequencies and as for the short chamber example the most accurate prediction is given with the 30 mm mesh. Moreover it can be noticed as also seen in figure 45 that in the range at 1500 Hz to 3000 Hz the 30 mm mesh predicts the overall damping level whereas the 40 mm mesh is overpredicting this level. Unfortunately the 20 mm mesh has similar numerical miscalculations as the previous muffler type as seen in figure 35.

does not deliver any usable results as also observed for the previous muffler.

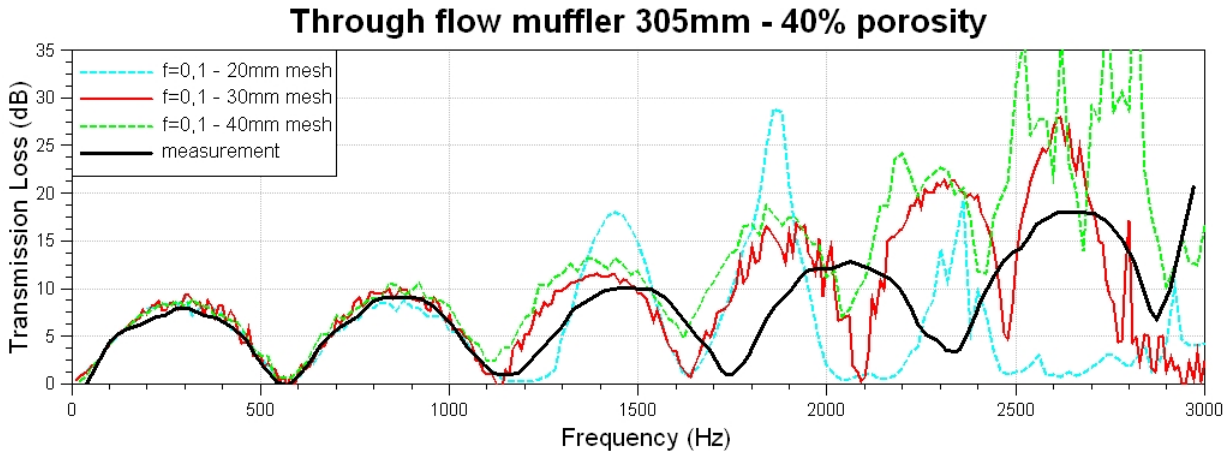

Figure 44 – Test case with pipe A - high porosity - different 3D cell sizes

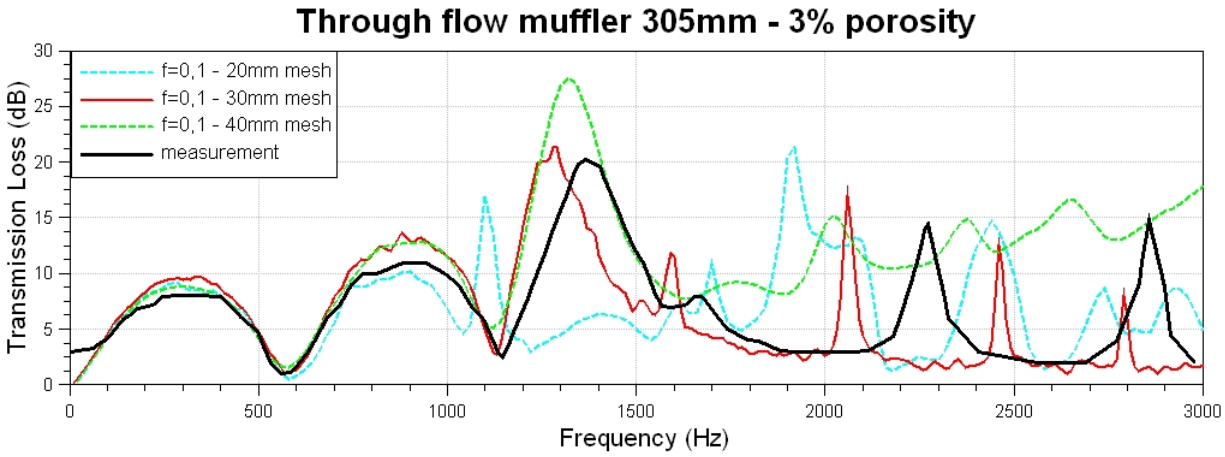

Figure 45 – Test case with pipe C - low porosity - different 3D cell sizes

Results and discussion

In figures 46, 47 and 48 simulations were done with different friction factors. For best possible prediction the 30 mm mesh was used. As the arrows indicate with increasing friction factor f the transmission loss increases but for the peaks at around 1500 Hz (figure 46), 1400 Hz (figure 47) and 1600 Hz (figure 48) the transmission loss is decreasing with increasing friction factor. This smoothing effect was also observed for the through flow muffler with the shorter chamber. Further it can be seen that the damping behaviour is getting worse with decreasing porosity. Several peaks at around 1700 Hz, 2300 Hz and 2900 Hz are also predicted with a frequency shift to lower frequencies. For simulation results here a friction factor about $f = 0.1$ fits the measurements best.

Figure 49 illustrates simulation results with different porosity levels and its influence on the transmission loss behaviour. Beginning with 80 % which would be very similar to an empty chamber the porosity level is decreased down to 3 %. The graph shows for the 80 % case that the second circumferential mode at 2921 Hz is excited (m=2, n=0). With decreasing porosity level this higher order mode peak is shifted to lower frequencies as the red line indicates. This leads to the assumption that the peaks at around 1500 Hz in figures 46, 47 and 48 are a shifted version of the second cicumferential mode.

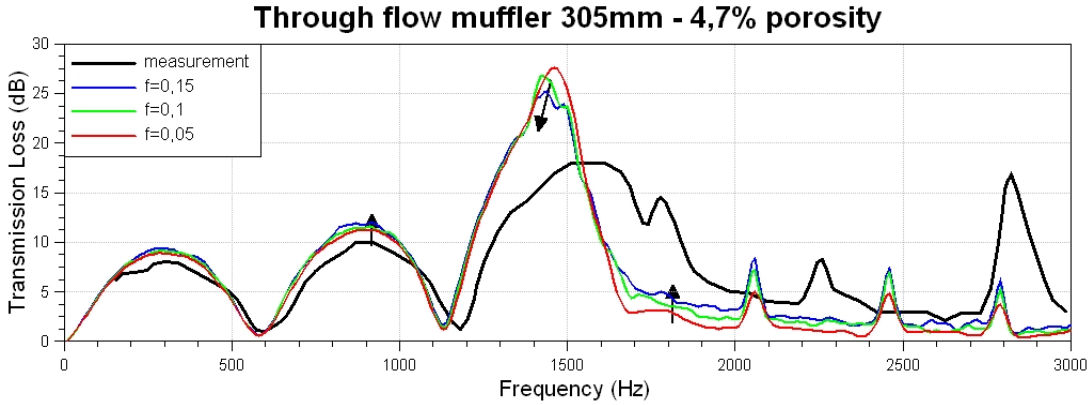

Figure 46 – Test case with pipe B

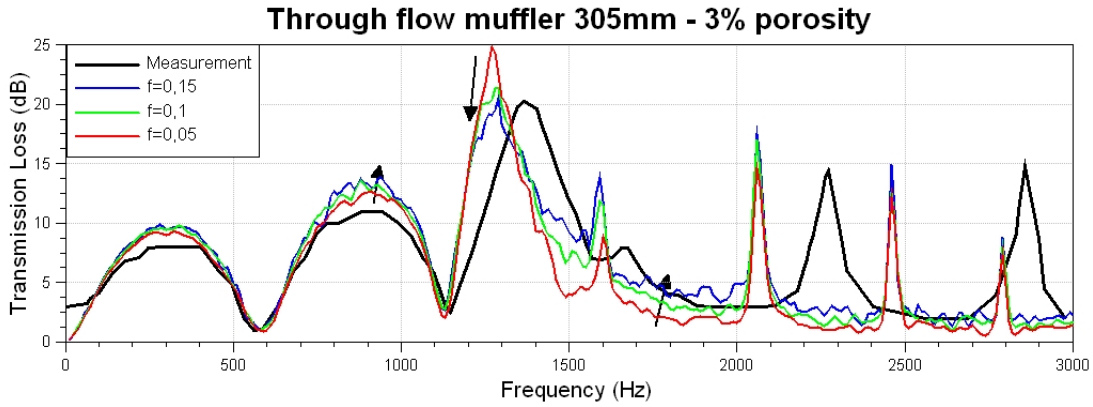

Figure 47 – Test case with pipe C

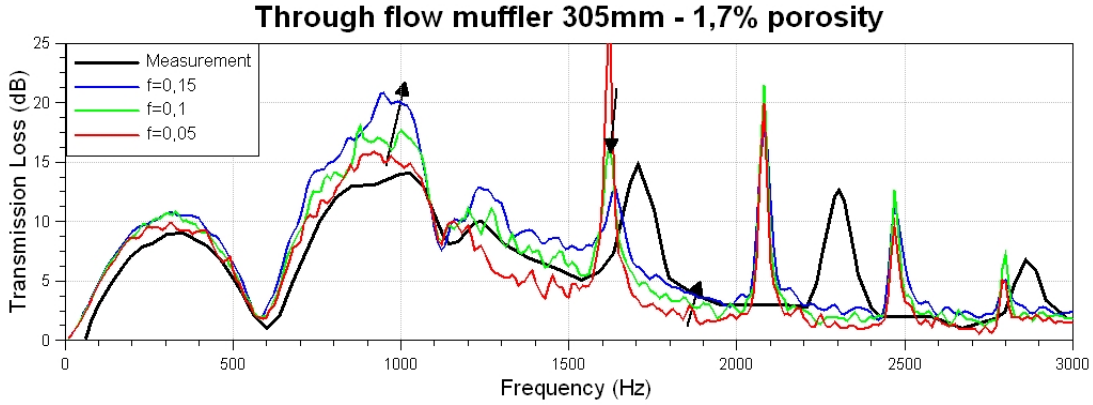

Figure 48 – Test case with pipe D

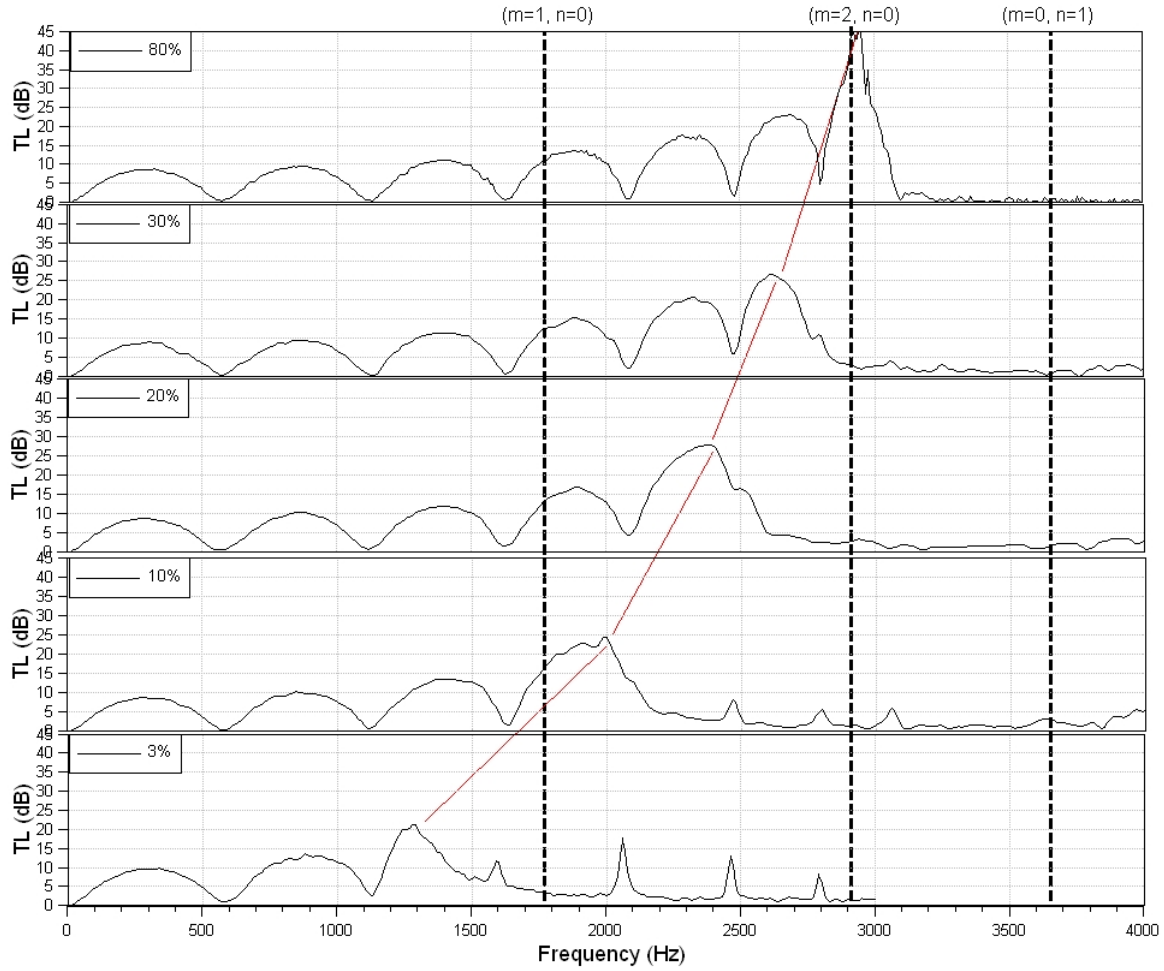

Figure 49 – Influence of the perforated pipe on the acoustic behaviour with decreasing porosity level

4.2 Plug mufflers

The acoustic performance without mean flow and with mean flow of four plug muffler configurations are investigated. The tested muffler types are a *Single plug muffler*, *Double plug muffler*, *Eccentric plug muffler* and a *Two chamber eccentric plug muffler*. For the first three muffler types also the pressure loss is investigated. Experimental measurements of the transmission loss and pressure loss are taken from reference ICSV 15 [35], except the measurements for the "two chamber eccentric plug muffler" which are done at AVL Graz. For the single plug and the eccentric plug muffler some transmission loss results are also compared with one-dimensional simulation results done with "AVL BOOST Linear Acoustics" [1]. As for the through flow mufflers simulations with different friction factors for the perforated connector are done and commented.

Simulation results with flow are accomplished as the mean pressure at system boundary 1 is at a higher level than the mean pressure at system boundary 2, so that a pressure difference causes a flow through the muffler and the according Mach number is achieved.

4.2.1 Single plug muffler

The inner diameter for this muffler is 197 mm, the length is 205 mm, the inner diameter of the perforated pipe and the inlet and outlet pipe is 57 mm. This is pictured in figure 50. The perforated pipe is separated in the middle with a plug of 15 mm length, so that the steaming air flow is forced through the perforation. Two different porosity levels for the perforated pipe are investigated: 5% porosity with $d_h = 5$ mm and 12% porosity with $d_h = 4$ mm.

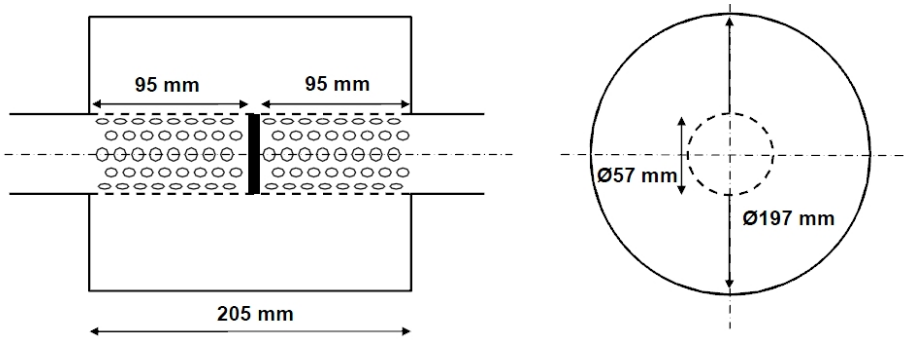

Figure 50 – Scheme: Single plug muffler [35]

In figure 51 the 3D cell mesh model in Boost is shown. It consists of 224 3D cells for the cavity and 14 cells straight in a line for the perforated pipe. The approximate sidelength of the mesh / 3D cell is 30 mm. Other meshes with 20 mm and 40 mm also have been tested, but with worse results for the transmission loss, comparable to those obtained for the through flow muffler in chapter 4.1.

The sum of all 3D cells model the total volume of the muffler accurately. Each cell of the perforated pipe is connected to the surrounding cavity due to four perforated elements.

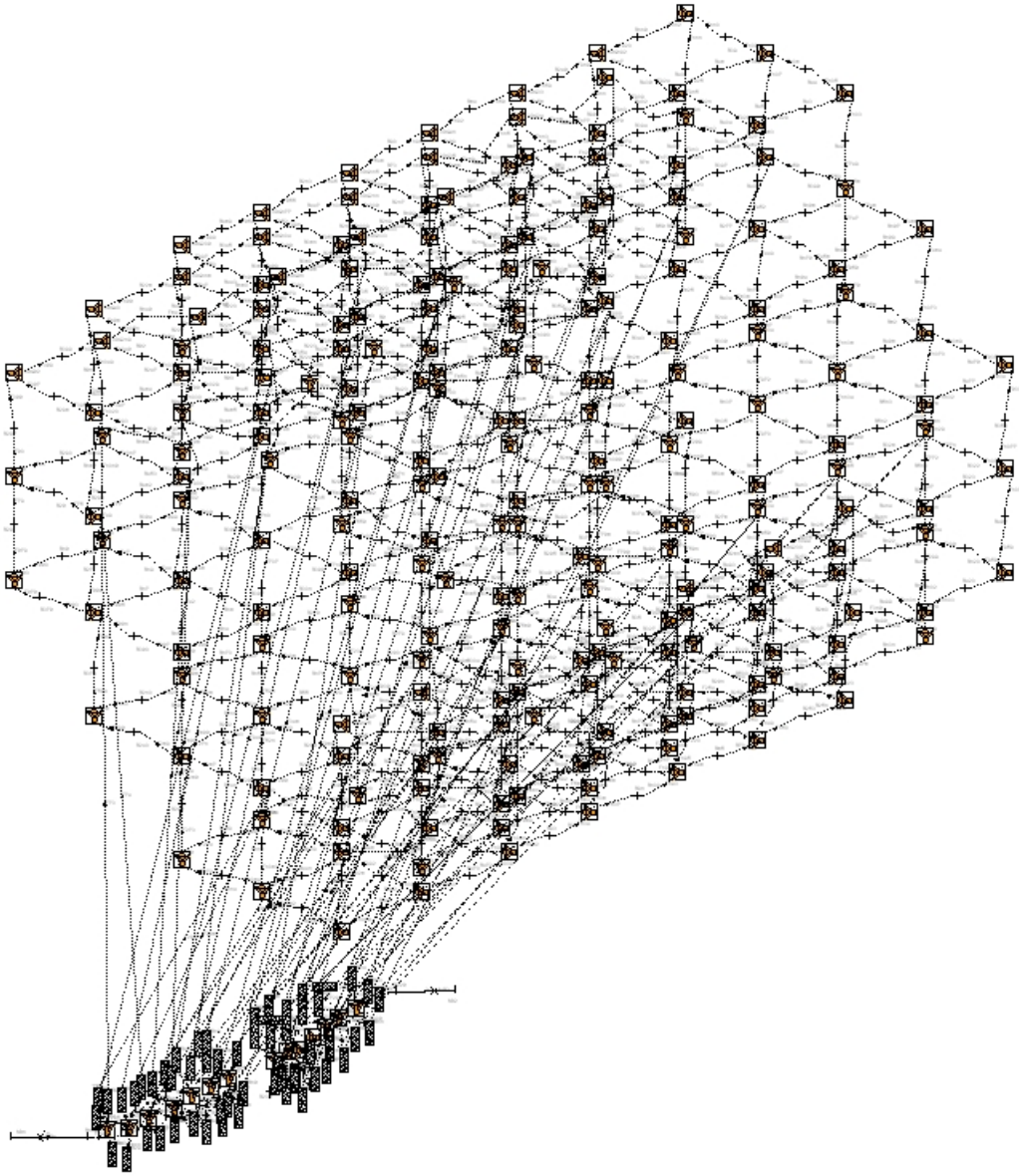

Figure 51 – Single plug muffler model (Boost GUI)

Results and discussion

Pressure loss: As also the performance of the muffler is of interest pressure loss measurements are compared to simulations with different friction factors. To find out the best matching friction factor those simulations are done before acoustic simulations. As seen in figure 52 for different porosity levels a friction factor between f=0.25 and 0.3 fits the measurements best.

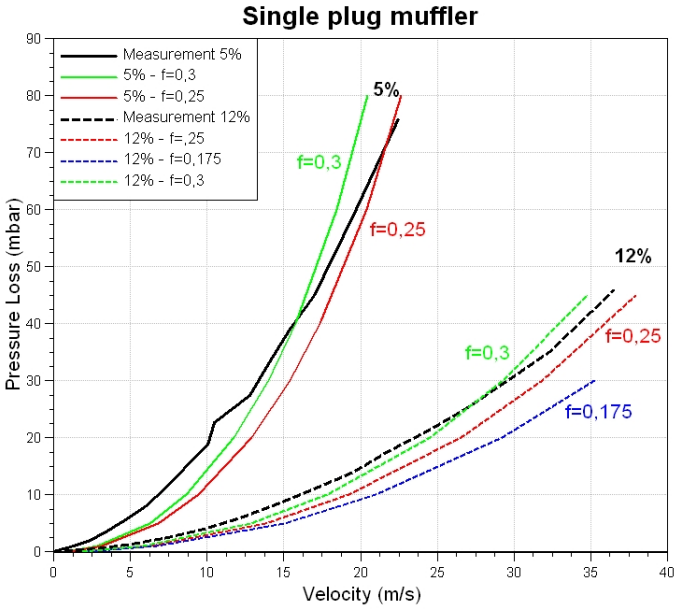

Figure 52 – Measurement vs. simulation for 5 % and 12 % porosity with different friction factors

Transmission loss: To find out the best size for spatial pipe discretisation of the inlet and outlet pipe, different values are tested as seen in figure 53. 10 mm give the lowest overprediction and the smoothest result. Also the computational time is the shortest in this case. This does not agree with results from chapter 4.1, see figure 34, where the computational time is increasing with smaller pipe discretization.

In figure 54 the influence of the end correction length coefficient α, which is influencing the imaginary part of the perforated impedance, is shown. It can be seen that the damping is decreasing slightly and the higher order peak is shifting to higher frequencies with decreasing α.

The influence of the plug in the middle of the perforate pipe on the damping behaviour is seen in figure 55. For low frequencies up to 850 Hz the transmission loss is lower with the plug, but above 1100 Hz the transmission loss is improved with the plug. This might be due to the increased dissipative character when the sound waves are forced through the perforation. The improvement in sound attenuation has its drawback in the increase of the pressure loss across the muffler.

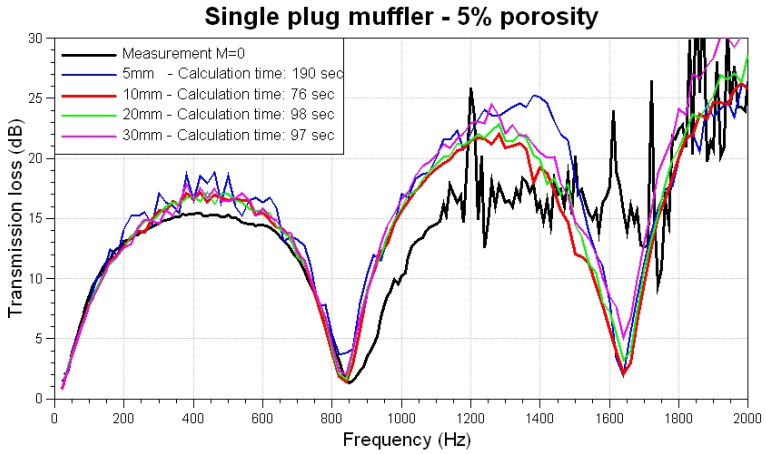

Figure 53 – Influence of different spatial pipe discretization and the according calculation times with 10 cycle simulation

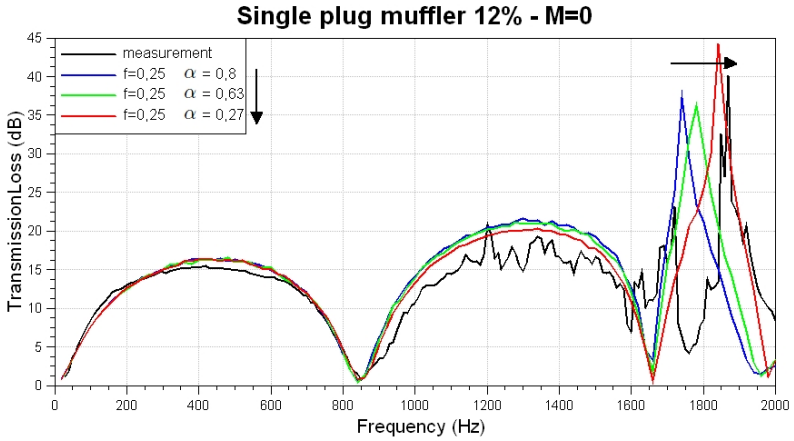

Figure 54 – Influence of different end correction length coefficients α with constant friction factor

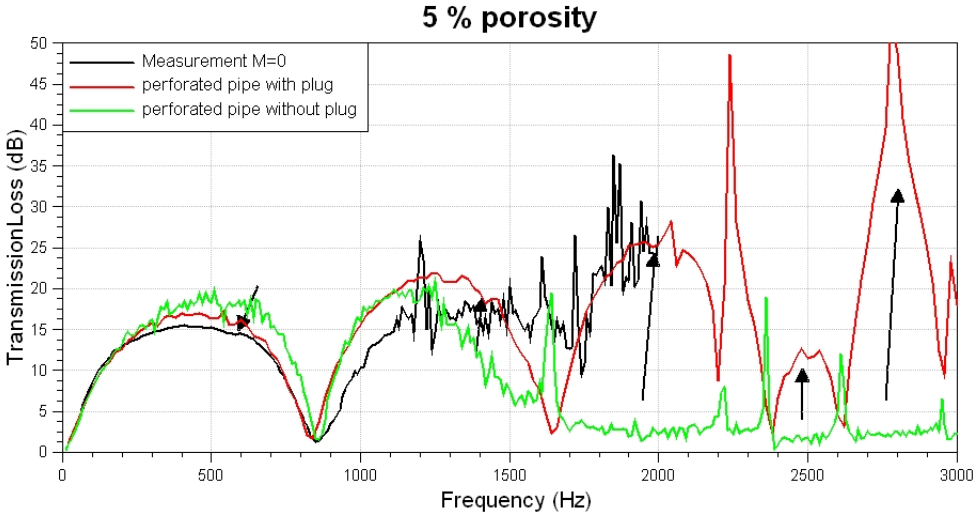

Figure 55 – Influence of the plug for zero mean flow M=0

Simulations of the transmission loss, with friction factors corresponding to the results from pressure loss simulations, are compared with measurements in figure 56 for 5 % porosity and in figure 57 and 58 for 12 % porosity. In figure 58 the 3D cell simulation result is compared with a one-dimensional simulation result carried out with "AVL BOOST Linear Acoustics" [1]. It can be observed that the higher order mode peak is captured with the 3D cell approach, even if shifted in frequency, but with the one-dimensional approach it is not captured.

According to simulation results the friction factor has more influence for the simulations with flow and the lower porosity case with 5 % porosity than to 12 %. Simulation results without mean flow (M=0) for both porosity levels give good agreement with the measured data up to 850 Hz. Aboth this frequency the damping is overpredicted and due to the limiting accuracy of the mesh size (30mm mesh) (compare also to the 40mm mesh figure 54) a frequency shift occures as already observed for the through flow muffler in chapter 4.1. As mentioned before best results where done with a 3D cell size of 30 mm. Unfortunately a more accurate mesh size of 20 mm does not lead to a more accurate solutions. For all simulations it seems like a friction factor around f=0.25 fits the measurements best.

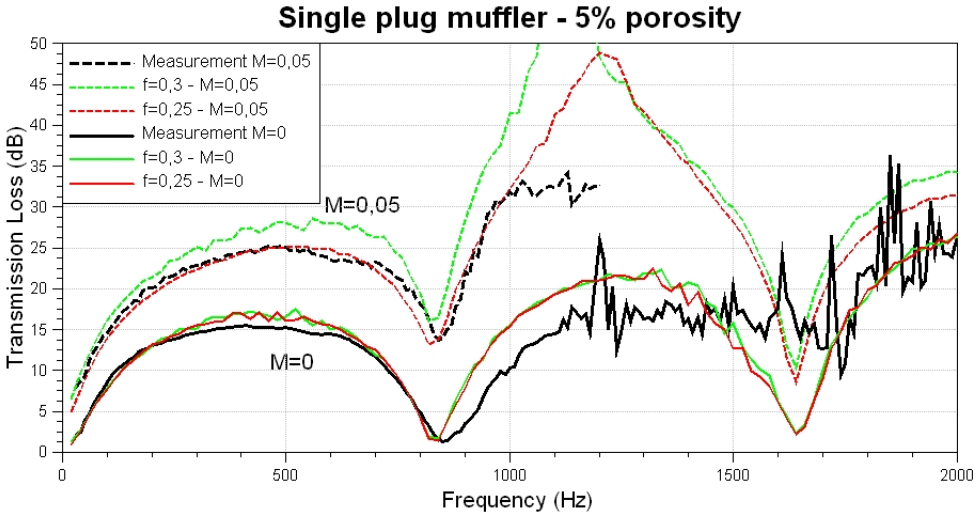

Figure 56 – Test case with 5 % porosity

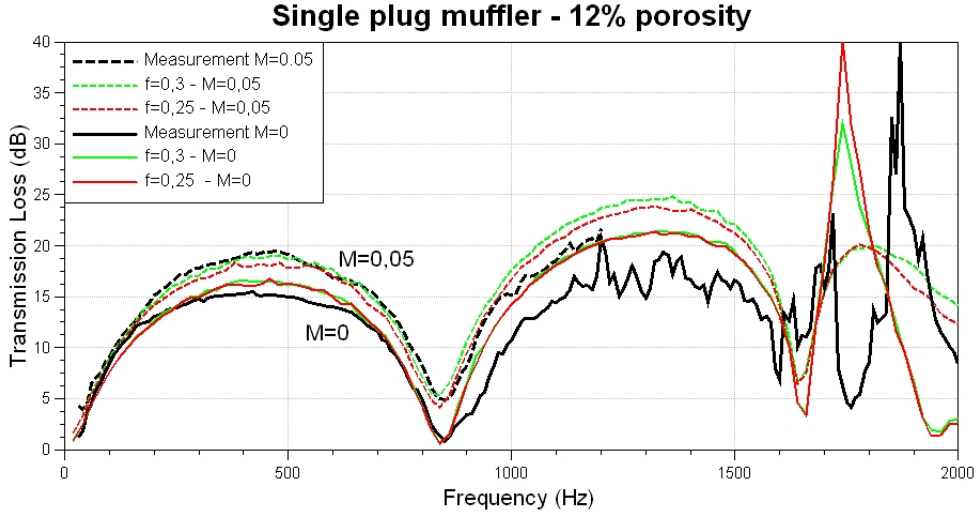

Figure 57 – Test case with 12 % porosity

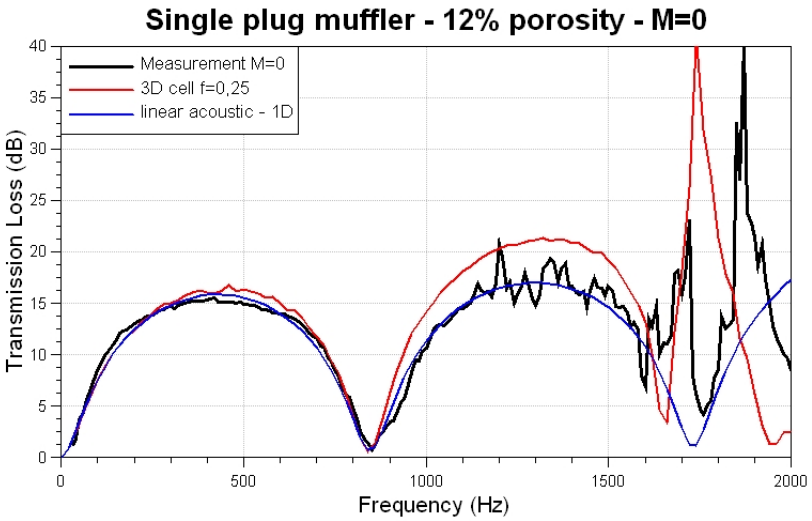

Figure 58 – Comparison 1D linear acoustic with 3D cell approach

Higher order mode effects: Due to the concentric geometry the first circumference mode is not excited but the first radial mode at $f = \frac{3{,}83c}{\pi D}$ where c is the speed of sound and D the diameter of the chamber would lead to a frequency f=2123 Hz. This value is valid for empty chambers, however for mufflers with perforated pipes this peak is shifted to lower frequencies. This can be observed for the 12 % porosity muffler in figure 57 at around 1900 Hz for the no flow case for both measurements and simulation results. For the flow case the measurement is just valid up to 1200 Hz, but the simulation also shows up with a smoothed peak. This also can be observed later for the eccentric plug muffler in chapter 4.2.3. For the 5 % porosity muffler this first radial mode is expected to occure at an even lower frequency but because it is very likely overlapped with the second maximum it is not obviously visible in the result. This can be observed at figure 59 where simulations with different porosity levels are compared to each other. As mentioned before the peak of the first radial mode is shifting to lower frequencies as the porosity decreases.

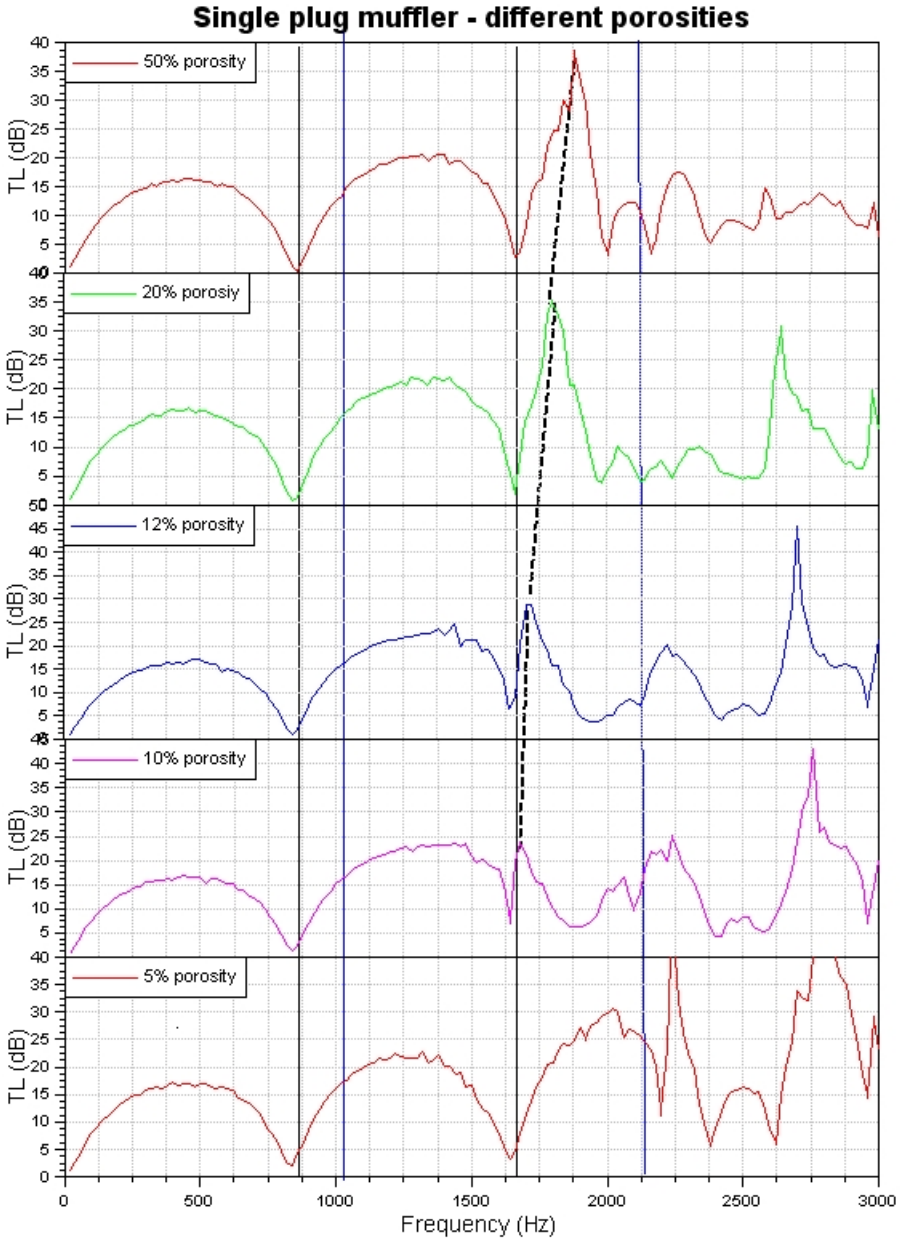

Figure 59 – Simulation results with different porosity levels

4.2.2 Double plug muffler

The double plug muffler consists of two single plug mufflers in a row which are separated due to a 2 mm thick wall. The total length of the muffler is 257 mm, the chambers diameter is 197 mm, the inner diameter of the perforated pipe an the inlet and outlet pipe is 57 mm. The hole diameter d_h for all porosity levels is 4 mm and wall thickness of the perforated pipe is 1.2 mm.

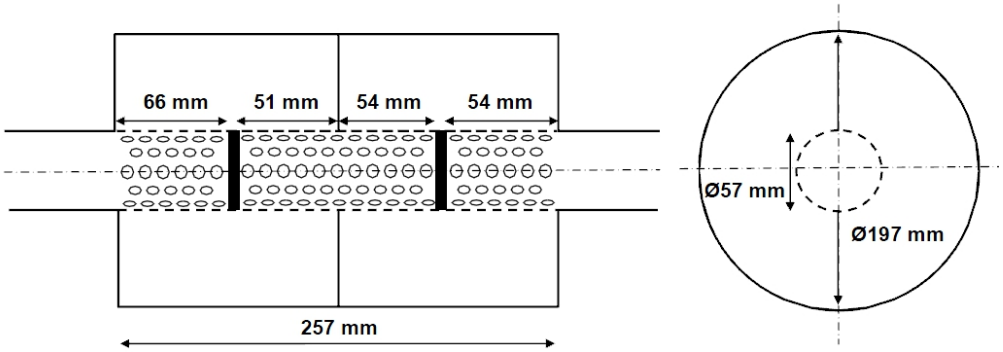

Figure 60 – Scheme: Double plug muffler [35]

Comparison of the double plug with the single plug muffler leads to the following statements:

- Due to the increase of volume the attenuation behaviour is increased.
- The fluid flow has to pass approximately double the amount of perforates, therefore the pressure loss is increased. For approximately the same pressure loss as for the single plug muffler the porosity has to be much higher. This can be seen when comparing the pressure loss for 12 % porosity in figure 52 for the single plug muffler with the pressure loss for 28 % porosity for the double plug muffler in figure 64.
- Resonance frequencies cannot be calculated as for a simple expansion chamber. The damping behaves more like the summation out of the damping behaviour of the two chambers, which can be seen in figure 62. Though the drops in the summation at the marked areas in the graph do not occur from the summation but are typical characteristics of the double plug muffler.

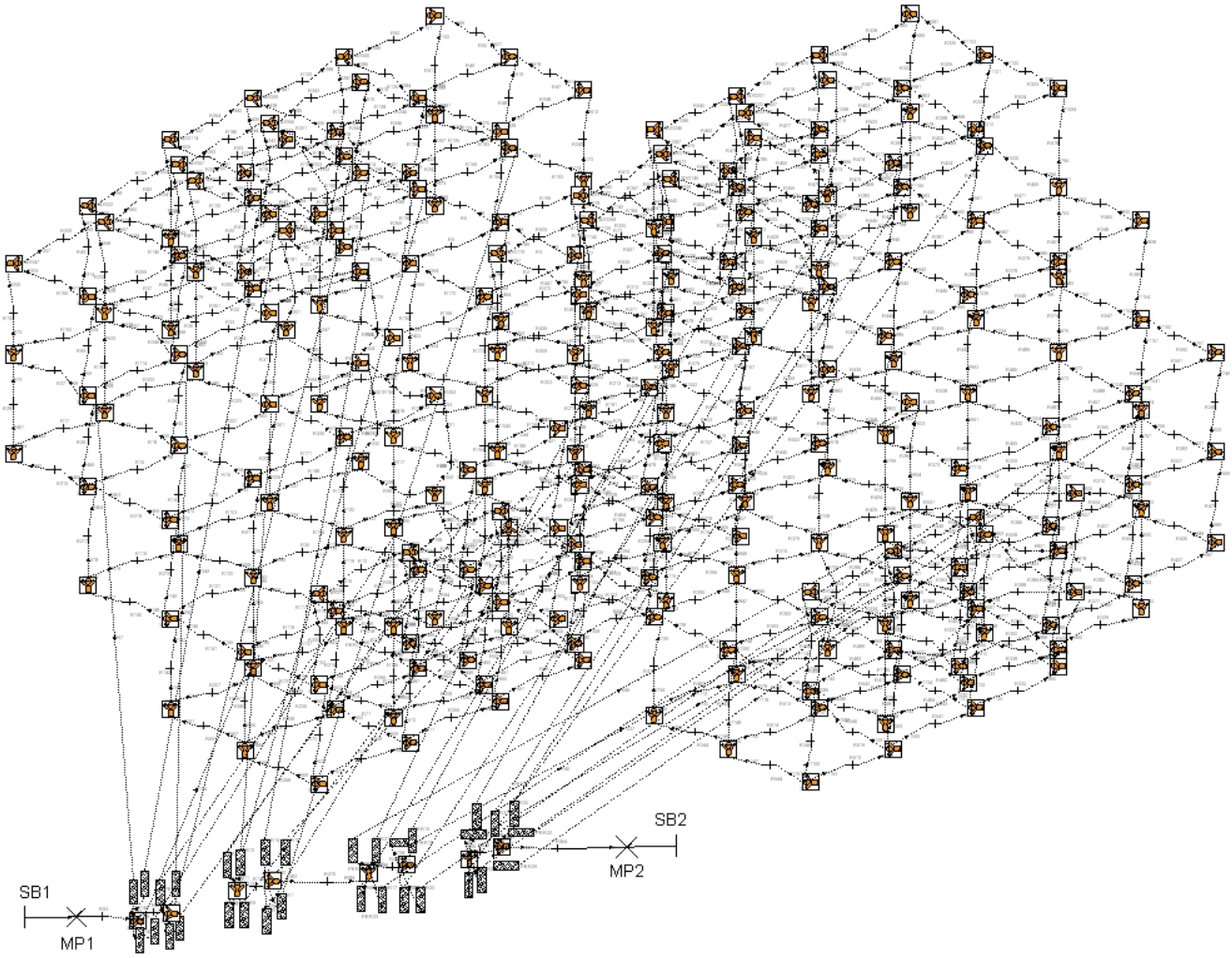

Figure 61 – Double plug muffler model (Boost GUI)

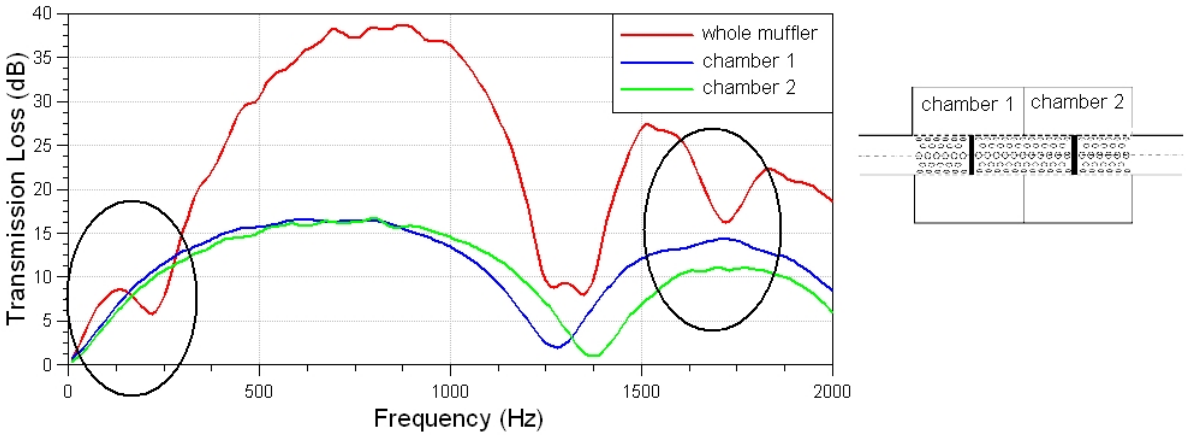

Figure 62 – Summation of the attenuation in chamber 1 and chamber 2 with 7 % porosity level of the perforated pipe without mean flow

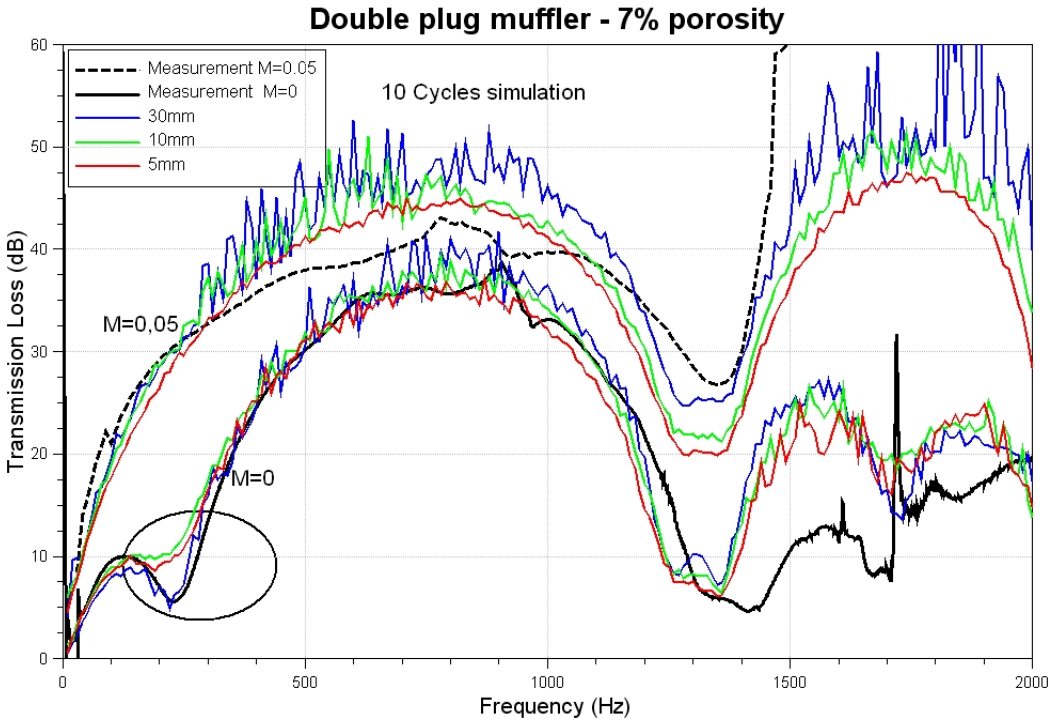

Figure 63 – Influence of the spatial pipe discretization, all results with $f = 0.15$

The 3D cell mesh consists out of 264 3D cells where the outer chamber is modelled with 256 cells and the perforated pipe with 8 cells. The approximate sidelength of the mesh is 30 mm and the spatial pipe discretization is 5 mm for all simulation results. This is compared to other values of the spatial pipe discretization as shown in figure 63, where the results with 5 mm give the less fluctuation and the less overprediction. The drop at around 250 Hz is best captured with 30 mm pipe discretization. Unfortunately this effect could not be investigated further within the scope of this thesis.

Results and discussion

Pressure loss: The comparison of measurements with simulation results with different friction factors can be seen in figure 64. Simulation results with a friction factor of $f = 0.2$ give good agreement with measurements for a porosity level of 28 %, but for 14 % it is slightly overpredicted and for 7 % even more. For 14 % a friction factor between $f = 0.15$ and 0.2 and for 7 % between $f = 0.1$ and 0.15 would fit the best the measurements.

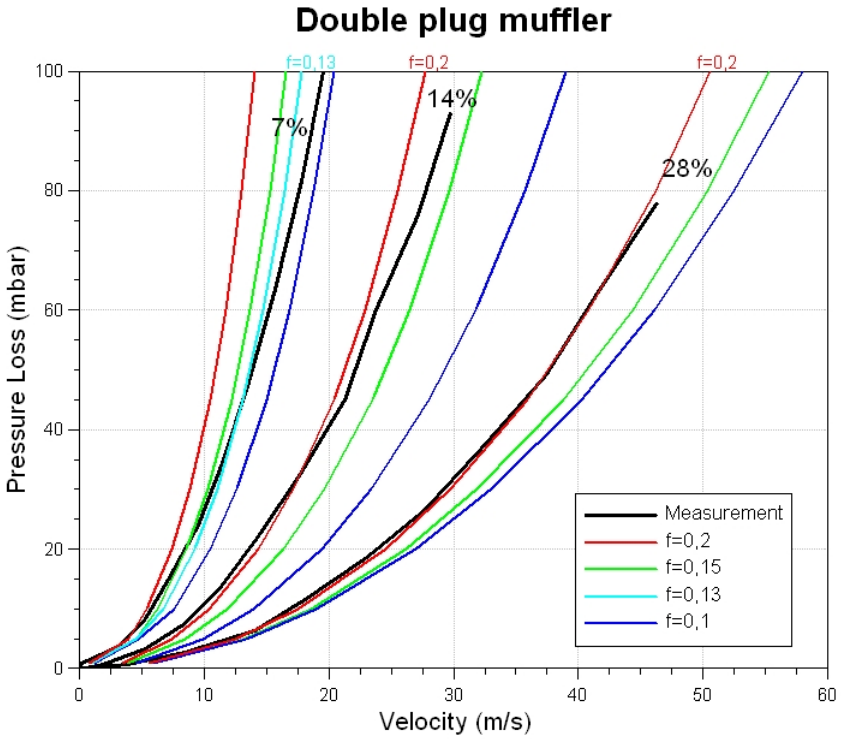

Figure 64 – Measurement vs. simulation for 7 %, 14 % and 28 % porosity with different friction factors

Transmission loss: In figures 65 - 67 result with different porosity levels without flow and with flow are shown. The spread of simulation results with flow and with different friction factors is much higher for low porosity levels. It can be seen that transmission loss simulations show the best agreement with measurements with the same friction factors as for the pressure loss simulations.

For simulation results **with flow** for the 7 % porosity case the simulation results with a friction factor between $f = 0.1$ and 0.15 would fit the measurements best, whereas for the 14 % porosity case the fricton factor would be between $f = 0.15$ and 0.2. For the 28 % porosity case the friction factor does not have that great influence, but at the drop around 250 Hz it can be seen that $f = 0.2$ would fit the measurement best.

For simulation results **without flow** the transmission loss is predicted very well and the friction factor does not have that great an impact on the results as the simulations with flow. Above 1300 Hz the solution shows an overestimation of around 10 dB for all porosity levels without flow.

For all results the minimum at 1400 Hz is captured with a frequency shift to lower frequencies whereas the drop at around 250 Hz is captured quiet well for the higher porosity level but for the 7 % case it is not captured entirely.

The required number of cycles for all porosity cases for the no flow case is 10 cycles which requires about 5 - 6 minutes calculation time, whereas the flow case simulation requires 30 cycles, with a calculation time about 15 minutes, for an accurate solution. It can be seen that for 7 % porosity even more cycles would be required whereas for the higher porosity levels 30 cycles were sufficient.

In general the transmission loss and pressure loss increase with decreasing porosity level of the perforation.

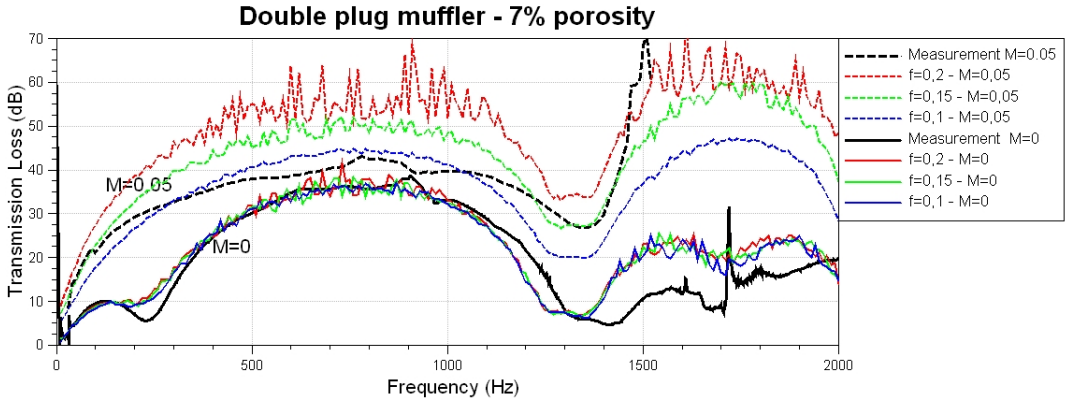

Figure 65 – Test case with 7 % porosity

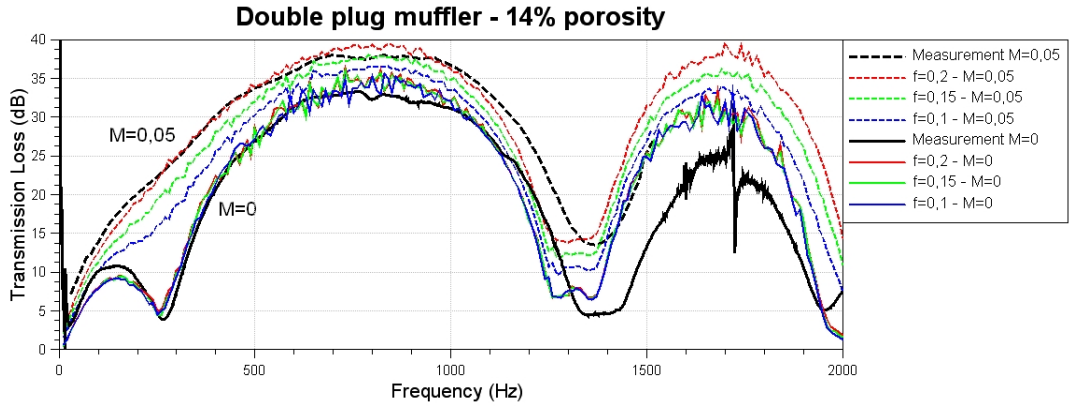

Figure 66 – Test case with 14 % porosity

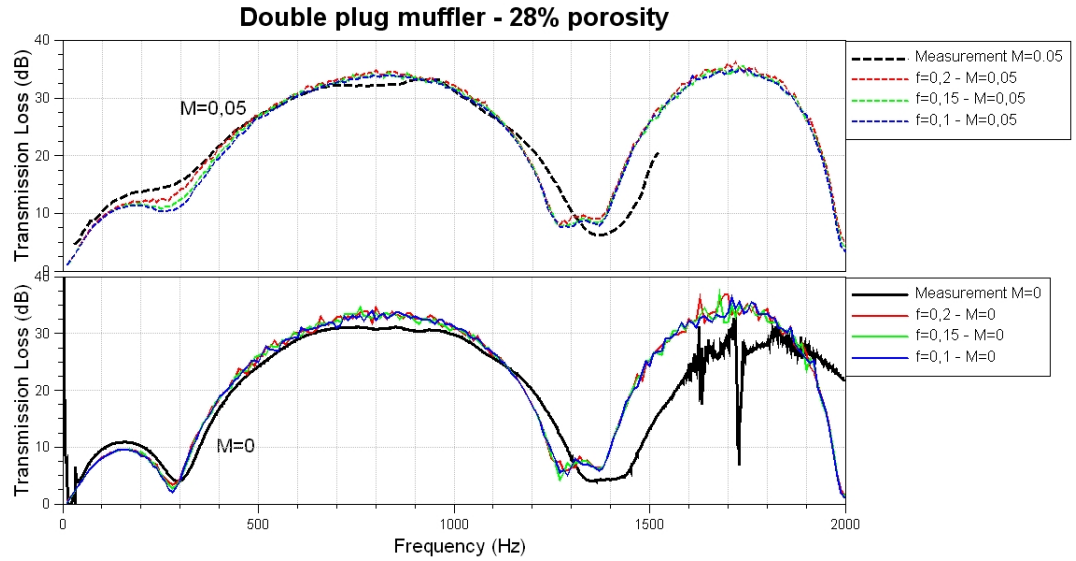

Figure 67 – Test case with 28 % porosity

4.2.3 Eccentric plug muffler

The eccentric plug muffler consists of a chamber with two perforated pipes which are applied asymmetrically to the chamber. The perforation is constant for the whole length of the pipes. Flow is forced out through the perforated holes of the inlet pipe and in through the perforated holes of the outlet pipe before exiting the outlet pipe itself [35]. Two different porosity levels for the perforated pipes are tested 5 % and 12 %.

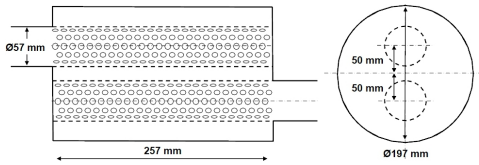

Figure 68 – Scheme: Eccentric plug muffler [35]

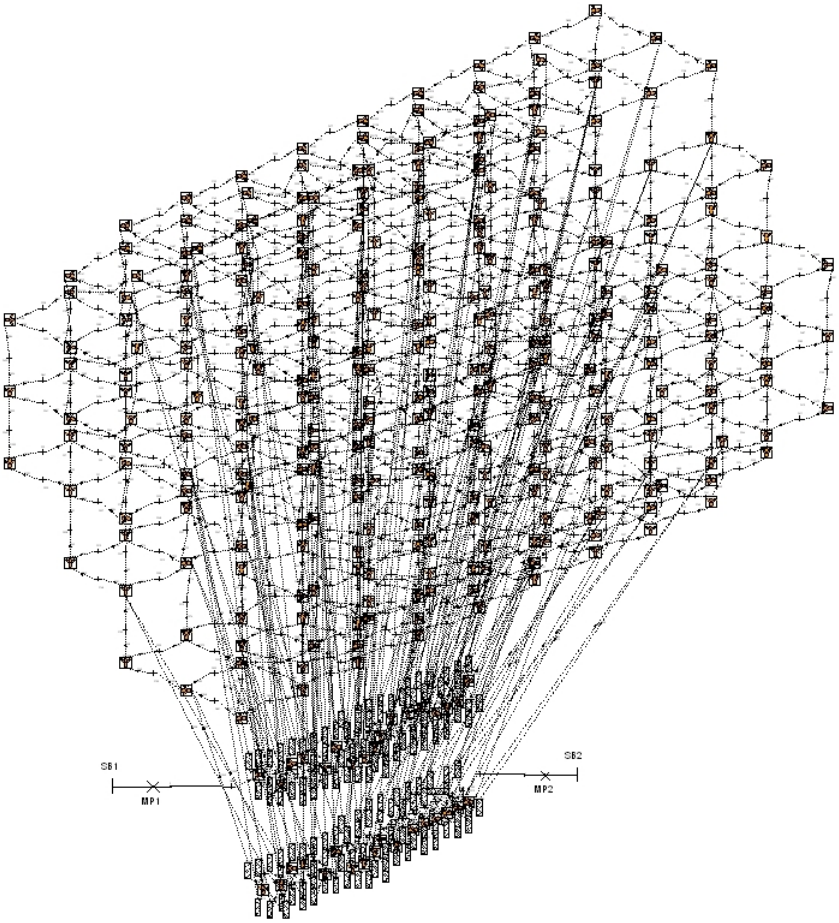

Figure 69 – Eccentric plug muffler (Boost GUI)

Results and discussion

Pressure loss: Simulations for the 5 % case show good agreement with a friction factor of $f = 0.25$ which also is in the range of the single plug and double plug muffler. A considerable discrepancy is observed for the pressure loss simulation for the 12 % case. A friction factor of $f = 0.055$ would fit the measurement best.

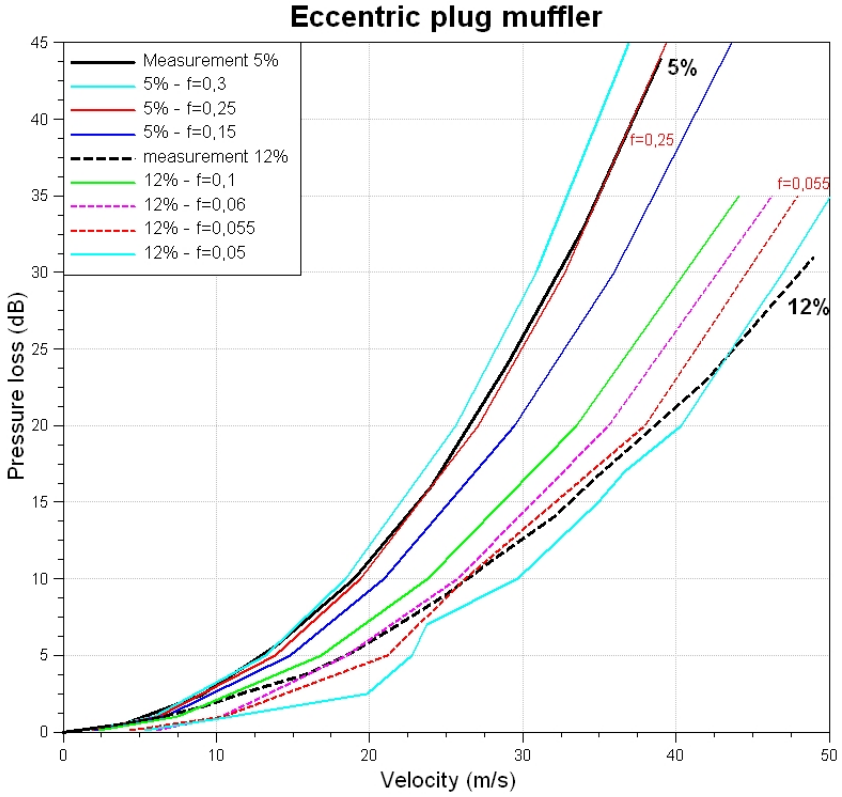

Figure 70 – Measurement vs. simulation for 5 % and 12 % porosity with different friction factors

Transmission loss: In figure 71 simulation results with different cell sizes are shown. For an approximate 3D cell side length of 40 mm a mesh out of 136 cells is required to model the muffler's volume. For 30 mm 331 cells, which is shown in figure 69, and for 20 mm 918 cells. In table 3 the computational times for the different meshes are listed for a 10 cycle simulation. The peak at around 800 Hz is not captured accurately by any of the different meshes. Different to all the examples before with increasing cell size the peak is shifting to higher frequencies (cf. figure 35, 45 and 54). One possibility is that

the limitation of the one dimensionality of the perforated pipes is limiting the accuracy for the eccentric plug muffler due to the diagonal flow direction through the perforated pipes.

mesh accuracy	number of 3D cells	spatial pipe discretization	computational time
40 mm	136	10 mm	33 sec
30 mm	331	10 mm	2 min 30 sec
20 mm	918	20 mm	13 min

Table 3 – Computational time for different 3D mesh accuracy for 10 cycle simulation

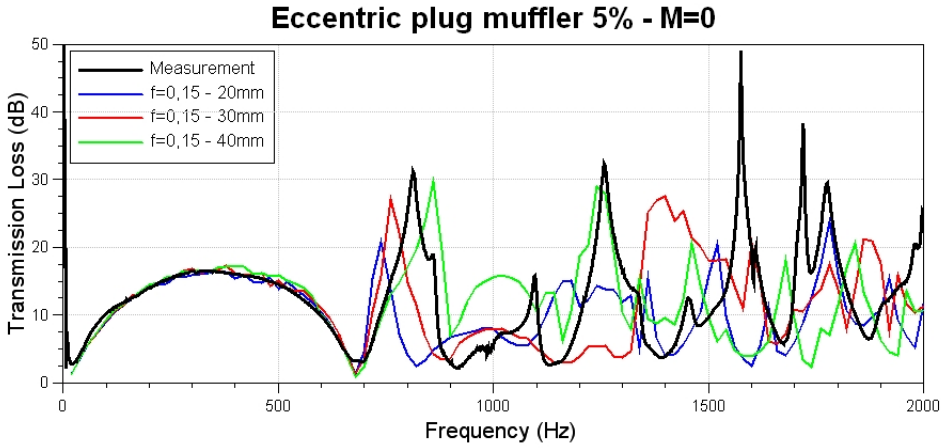

Figure 71 – Influence of different mesh size accuracies

The 30 mm mesh simulations with different spatial pipe discretizations deliver results as seen in figure 72. All results show an underestimation of the transmission loss. This is different to all simulation results obtained from the previous muffler types which usually overpredict the transmission loss. The behaviour that with smaller pipe discretization the damping decreases is constant with previous accomplished simulation result from other muffler types. Computational times for different spatial pipe discretizations are listed in table 4.

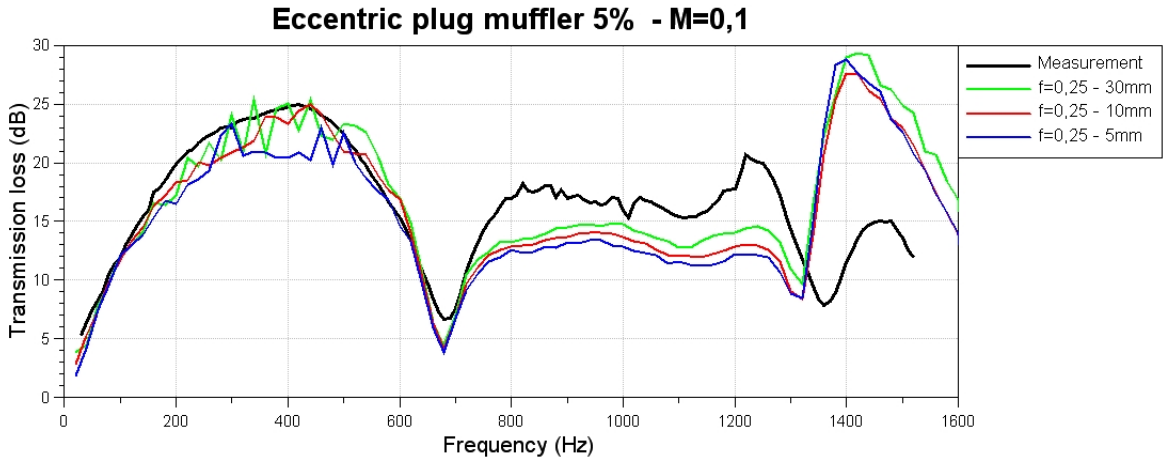

Figure 72 – Influence of the spatial pipe discretization

3D cell side length	spatial pipe discretization	computational time
30 mm	5 mm	7 min
30 mm	10 mm	4 min
30 mm	30 mm	4 min

Table 4 – Computational time for different spatial pipe discretization for 15 cycle simulation

Comparing the 5 % case with the 12 % case simulation it can be seen that the spreading of the curves with different friction factors is much higher with 5 % porosity, hence the friction factor has more influence when the porosity is low. This can be seen clearly for the simulation with flow in figures 74 and 76. It also can be seen that the same friction factor which fit best to the pressure loss results also fit best to the transmission loss results. E.g. the 12 % case, which is an exception because a very low friction factor of f = 0.055 would fit best to the pressure loss results, also fits the measurement best for the transmission loss with the same friction factor. Further in figures 73 - 76 the results from the 3D cell approach are compared to simulation results obtained with one-dimensional BOOST Linear Acoustics [1]. The 1D approach obviously shows poor prediction of the transmission loss above around 700 Hz, where the 3D cell approach delivers much better results.

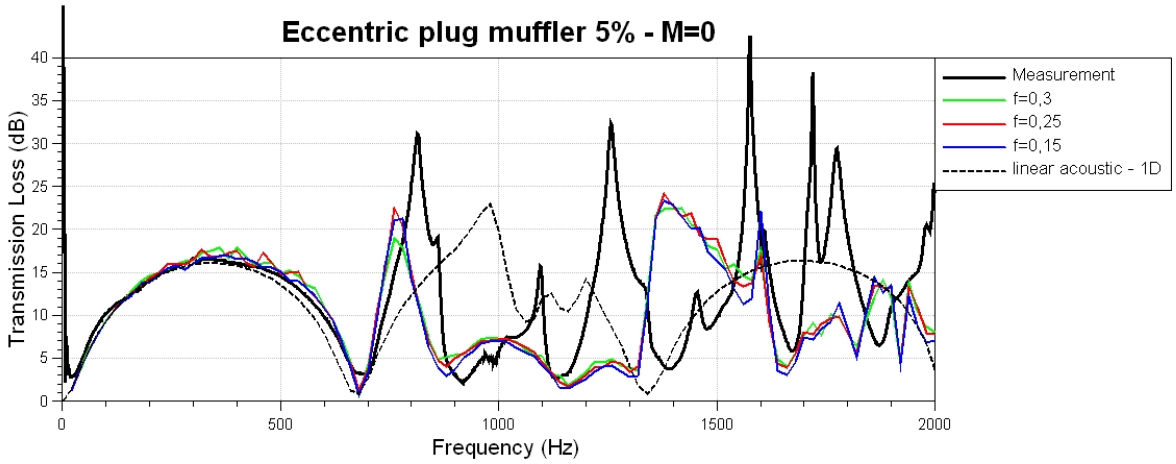

Figure 73 – Test case with 5 % porosity - without mean flow

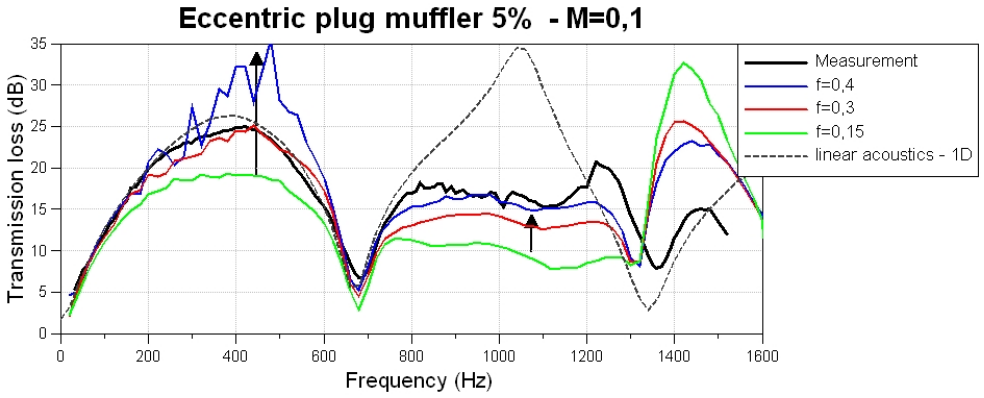

Figure 74 – Test case with 5 % porosity - with mean flow

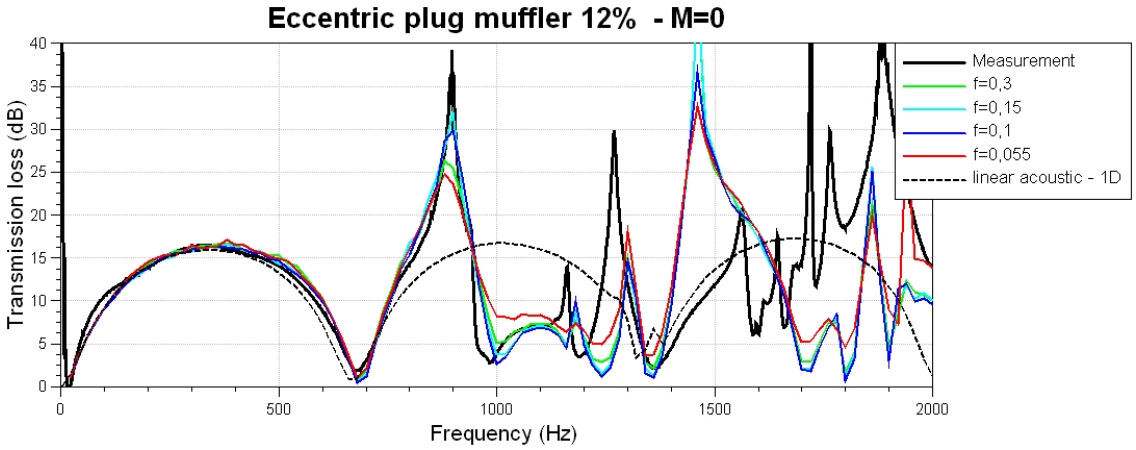

Figure 75 – Test case with 12 % porosity - without mean flow

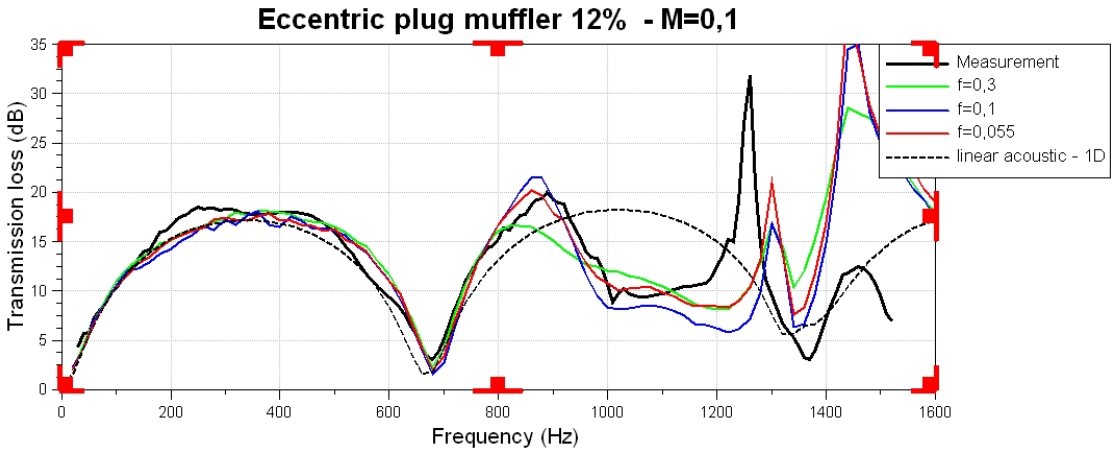

Figure 76 – Test case with 12 % porosity - with mean flow

4.2.4 Two chamber eccentric plug muffler

A more complex eccentric plug muffler is investigated. It consists of two chambers which are separated by a solid wall. The connection between those two chambers is created by the inlet and outlet pipes which are extended so that they reach into both chambers. Both pipes have two perforated sections with a high porosity at around 24 % and a plug at the end of the pipes. The flow is seperated in two streams where the first goes into the first chamber from perforation **1** to perforation **3** and the second one in the second chamber goes from perforation **2** to perforation **4**.

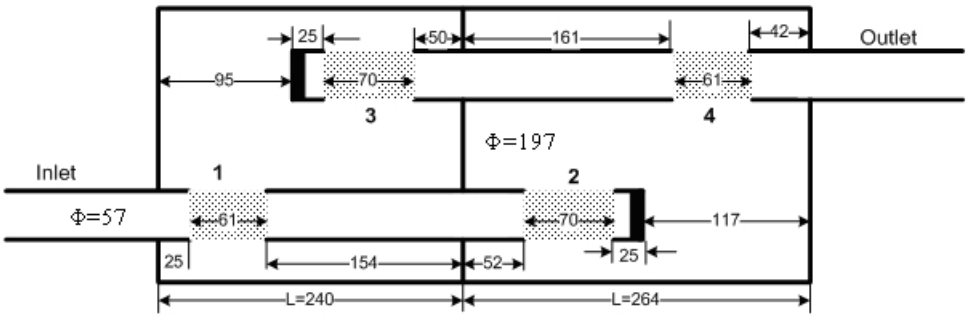

Figure 77 – Scheme: Two chamber eccentric plug muffler

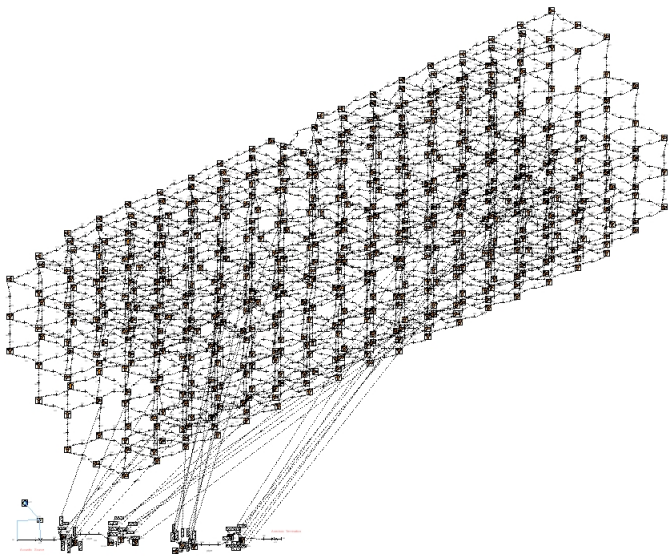

Figure 78 – Two chamber eccentric plug muffler in Boost

Mesh generation: The generated mesh consists out of 585 cells where a single 3D cell is approximately 30 mm. As seen in figure 78 the perforated sections/pipes are pulled out of the chambers mesh and in figure 79 a more detailed view of how the perforations are modelled is shown. The perforations **1** and **4** with a length of 60 mm are modelled out of two 3D cells whereas the perforations **2** and **3** with a length of 70 mm require three cells. Each cell has four perforated connectors which connect the pipe to the outer chamber. The pipe sections which connects the two chambers are modelled as simple pipe elements with the appropriate diameters and lengths.

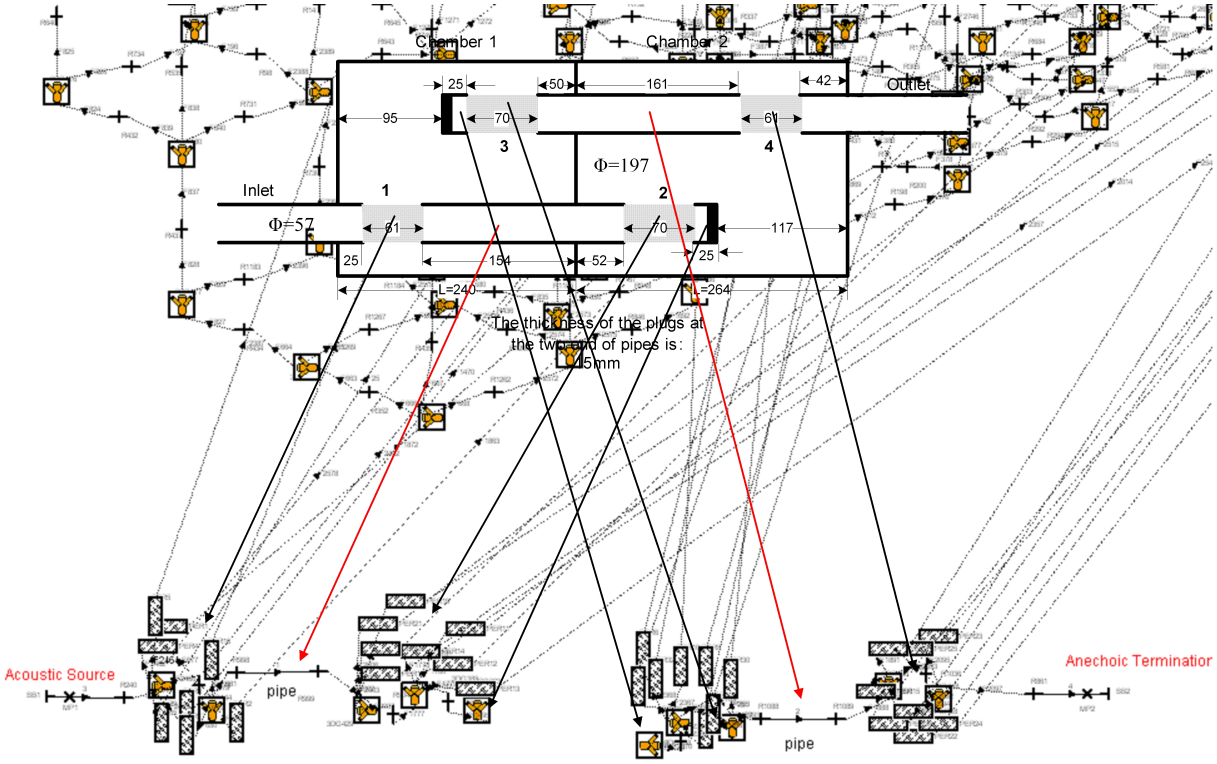

Figure 79 – detailed view of the modelling of the perforated sections

Results and discussion: The characteristic high damping level in the low frequency range from 200 Hz to 500 Hz comes from the chambers volume. Because of its separation into two chambers the maximums and minimums correspond to those chambers and the total transmission loss is more an overlap of the two chambers. As for the double plug muffler, also a drop at around 100 Hz can be observed for both the flow case and the no flow case. This low frequency drop is shifted to higher frequencies whereas over 400

Hz the simulation results shift to lower frequencies. This might be due to the limited accuracy of the generated mesh.

Simulations are done with three different friction factors $f = 0.15$, 0.2 and 0.3. For all simulation results a friction factor between $f = 0.15$ and 0.2 seems to be appropriate. Even for the flow case at M = 0.1 the friction factor does not have that much influence as in the previous examples. This can be explained by the high porosity level of the perforated sections and because the perforated areas are not that large.

It is conspicuous that in the frequency range from 200 Hz - 500 Hz and also for the peak at around 800 Hz the damping is increasing with decreasing friction factor.

Concerning the required cycles and calculation time the following is observed. For the no flow simulations 10 cycles are sufficient which requires around 9 minutes with a spatial pipe discretization of 10 mm. A decrease of the spatial pipe discretization to 5 mm has not lead to further improvement of the results but the calculation time is increased to 18 minutes. Simulation with flow requires approximately 1 minute longer.

For simulations with mean flow and with 10 cycles the result were very unstable hence simulations with mean flow were done with 25 cycles which require a calculation time of 22 minutes.

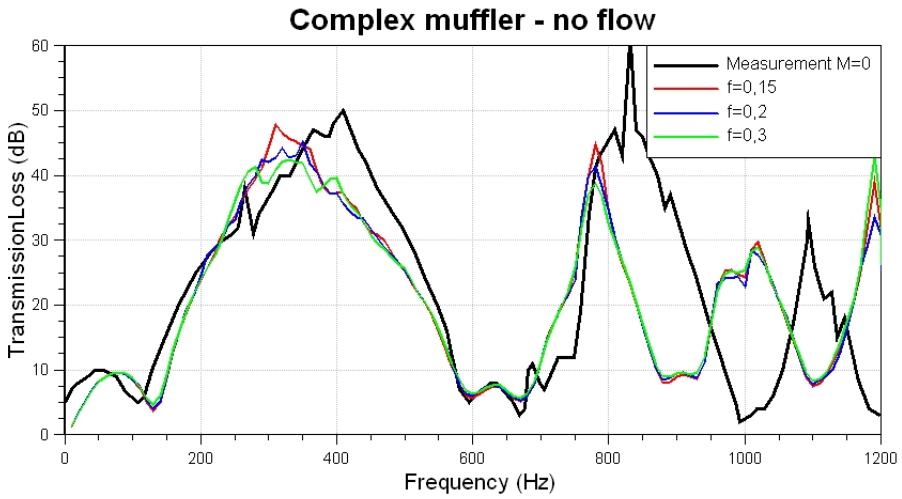

Figure 80 – Test case without mean flow

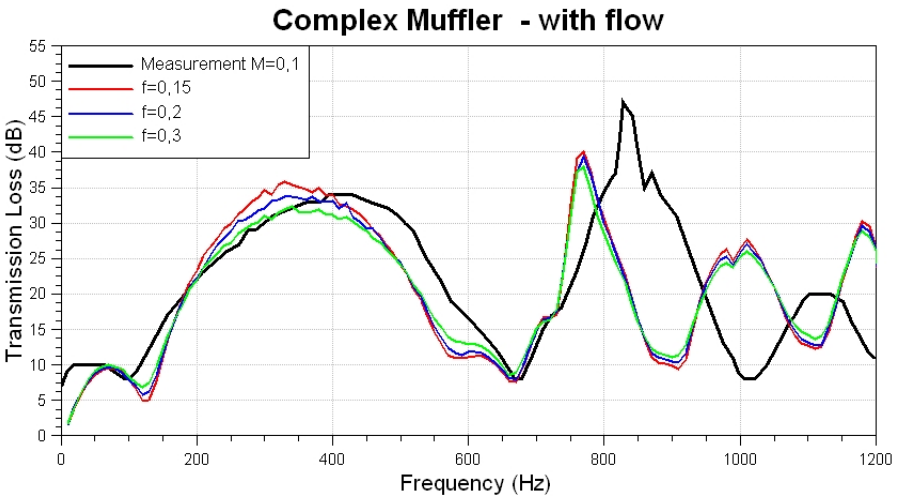

Figure 81 – Test case with mean flow - M = 0.1

5 Conclusion

5.1 Summary

The observations made from the transmission loss and pressure loss simulations of different muffler types, all containing perforated pipes, have come to the following conclusions.

The value of the friction factor is not constant for all muffler types but it can be stated that for perforations where the exhaust gas flow is mainly grazing the perforation, which is for through flow mufflers, the friction factor is between $f = 0.05$ - 0.15. For perforations where the exhaust gas flow is forced to stream through the perforations, which is for plug mufflers, the friction factor is between $f = 0.15$ - 0.3 . In other words the friction factor has to be set to a lower value for through flow mufflers and to a higher value for plug mufflers. For muffler examples for which pressure loss measurements were available (single plug, double plug and eccentric plug), the same friction factor which is valid for the pressure loss simulation, also is valid for the transmission loss simulation.

Changing the end correction coefficient α causes the higher order mode peak to shift in frequency. This peak shifts to higher frequencies with decreasing α. It also influences the pressure loss as with shorter end corrections, that means smaller values for α, the pressure loss is decreased. Usually the end correction coefficient is set to $\alpha = 0.8$, which is commonly used as a standard value for perforations.

Further the 3D cell size (discretization of the mufflers volume) has influence on the accuracy of the acoustic results, but nearly no influence on pressure loss results. As also observed for simulation results in foregone research [4] the transmission loss is predicted with a frequency shift to lower frequencies for all tested muffler types. This frequency shift decreases with smaller cell sizes and therefore the accuracy is increasing. Decreasing the 3D cell size from 40 mm to 30 mm leads to improvements for the accomplished results, whereat the calculation time increases with finer mesh dicretization.

Different spatial pipe discretization of the inlet and outlet pipe, which uses the one dimensional solver, also affects the accuracy and calculation time. Higher frequencies are affected more than lower frequencies. Several values are tested whereat 5 mm and 10 mm give best results, since the transmission loss is usually overpredicted and smaller pipe discretization yields to lower transmission loss especially above several hundred hertz.

It can be stated that with adequate parameter settings the transmission loss and pressure loss of automotive exhaust mufflers with perforated pipes can be predicted very good for low frequencies, but further improvements are necessary to enhance the accuracy for higher frequencies.

5.2 Outlook

Further investigations and developments on the subject are suggested, which are:

- Find a 3D cell size or rather a mesh size so that the frequency shift of the transmission loss might be avoided. Therefore the first step would be to solve the problems which occur with the 20 mm mesh.
- At present the modelling of the perforated pipe volume is limited to single cells arranged in a row. It is assumed that the accuracy especially for diagonal flow direction through the perforated pipe will increase with three dimensionality within the volume of the pipe.
- Implementation of an impedance model which distinguishes between grazing flow and through flow, which might be achieved with comparing the surrounding velocity vectors with the velocity through the perforation. This might lead to a solution where the friction factor could be kept constant.
- Further investigation on the behaviour of the end correction length coefficient α, especially concerning the distinction between grazing flow and through flow same as for the friction factor.
- Extension of the 3D cell solver to consider absorptive material behind the perforations to extend the simulation possibilities of the 3D cell approach.
- The present solution is solved in the time domain iteratively. One aim is to find a direct solver in the frequency domain for the 3D cell approach to shorten calculation times.

References

[1] *AVL BOOST Linear Acoustics User Guide, Edition 11, Version 2011.*

[2] R. Glav, "On acoustic modelling of silencers," *Department of Vehicle Engineering, Royal Institute of Technology, Stockholm, TRITA-FKT,*, vol. Report 9435, 1994.

[3] F. Karal, "The analogous acoustical impedance for discontinuities and constrictions of circular cross section," *The*, vol. 25, pp. 327–334, 1953.

[4] R. Fairbrother, S. Liu, and A. Dolinar, "Development of a generic 3d cell for the acoustic modelling of intake and exhaust systems," *International Congress on Sound and Vibration*, vol. 16, 2009.

[5] J. W. Sullivan and M. J. Crocker, "Analysis of concentric-tube resonators having unpartitioned cavities," *The Journal of the Acoustical Society of America*, 1978.

[6] K. Jayaraman and K. Yam, "Decoupling approach to modeling perforated tube muffler components," *The*, vol. 69(2), pp. 390–396, 1981.

[7] M. L. Munjal, K. N. Rao, and A. D. Sahasrabudhe, "Aeroacoustic analysis of perforated muffler components," *Journal of Sound and Vibration*, vol. 114(2), pp. 173–188, 1987.

[8] K. S. Peat, "A numerical decoupling analysis of perforated pipe silencer elements," *Journal of Sound and Vibration*, vol. 123(2), pp. 199–212, 1988.

[9] E. Dokumaci, "Matrizant approach to acoustic analysis of perforated multiple pipe mufflers carrying mean flow," *Journal of Sound and Vibration*, vol. 191(4), pp. 505–518, 1996.

[10] J. W. Sullivan, "A method for modeling perforated tube muffler components. i. theory," *The Journal of the Acoustical Society of America*, vol. 66(3), Sept. 1979.

[11] J. W. Sullivan, "A method for modeling perforated tube muffler components. ii. applications," *The Journal of the Acoustical Society of America*, vol. 66(3), Sept. 1979.

[12] E. Dokumaci, "A discrete approach for analysis of sound transmission in pipes coupled with compact communcating devices," *Journal of Sound and Vibration*, vol. 239(4), pp. 679–693, 2001.

[13] T. Elnady and M. Åbom, "On acoustic network models for perforated tube mufflers and the effect of different coupling conditions," *The Marcus Wallenberg Laboratory for Sound and Vibration Research, AVE, KTH*, 2004.

[14] P. O. A. L. Davies, M. F. Harrison, and H. J. Collins, "Acoustic modelling of multiple path silencers with experimental validations," *Journal of Sound and Vibration*, vol. 200(2), pp. 195–225, 1997.

[15] E. Dokumaci, "Effect of sheared grazing mean flow on acoustic transmission in perforated pipe mufflers," *Journal of Sound and Vibration*, vol. 283, pp. 645–663, 2004.

[16] J. H. Ferziger and M. Perić, *Computational Methods for Fluid Dynamics*. Springer, third, rev. edition ed., 2002.

[17] D. E. Winterbone and R. J. Pearson, *Theory of Engine Manifold Design*. Professional Engineering Publishing, London, 2000.

[18] D. E. Winterbone and R. J. Pearson, *Design Techniques for Engine Manifolds*. Professional Engineering Publishing, London, 1999.

[19] A. Onorati, "Prediction of the acoustical performances of muffling pipe systems by the method of characteristics," *Journal of Sound and Vibration*, vol. 171, pp. 369–395, 1992.

[20] A. Broatch, J. Serrano, F. Arnau, and D. Moya, "Time-domain computation of muffler frequency reponse: Comparison of different numerical schemes," *Journal of Sound and Vibration*, vol. 305, pp. 333–347, 2007.

[21] A. Onorati, "Nonlinear fluid dynamic modeling of reactive silencers involving extended inlet/outlet and perforated ducts," *Noise Control Eng. J.*, vol. 45 (1), pp. 35–51, 1997.

[22] A. A. El-Rahman, A. Abry, and A. Mobarak, "Non-linear simulation of single pass perforated tube silencers based on the method of characteristics," *Journal of Sound and Vibration*, vol. 278, pp. 63–81, 2004.

[23] G. Montenegro, A. D. Torre, A. Onorati, R. Fairbrother, and A. Dolinar, "Development and application of 3d generic cells to the acoustic modelling of exhaust systems," *SAE International*, 2011.

[24] M. Neffe, "Acoustic engine speed measurement," Master's thesis, Graz University of Technology, 2005.

[25] H. Klingenberg, *Automobil-Messtechnik*. Springer-Verlag, 2. edition, 1991.

[26] P. Zeller, *Handbuch Fahrzeugakustik*, vol. 1. Auflage. Peter Zeller, 2009.

[27] W. Weselak and G. Graber, *Raumakustik*, vol. Version 5.0. Institut für Breitbandkommunikation Technische Univeristät Graz, 2007.

[28] S. Kumar, "Linear acoustic modelling and testing of exhaust mufflers," Master's thesis, KTH, Stockholm, 2007.

[29] F. Fahy, *Foundations of Engineering Acoustics*. Elsevier Academic Press, 2001.

[30] T. Melling, "The acoustic impedance of perforates at medium and high sound pressure levels," *Journal of Sound and Vibration*, vol. 29(1), pp. 1–65, 1973.

[31] T. Elnady and H. Bodén, "On the modelling of the acoustic impedance of perforates with flow," Master's thesis, KTH, Stockholm, 2004.

[32] F. Payri, A. J. Torregrosa, and A. Broatch, "Pressure loss characterisation of perforated ducts," *SAE Technical Paper Series*, February 1998.

[33] H. Liu, S. Lu, and F. Zeng, "A study on the effects of higher order mode wave on mufflers performance," *Canadian Center of Science and Education*, vol. 1, pp. 170–175, 2009.

[34] L. J. Eriksson, "Higher order mode effects in circular ducts and expansion chambers," *The*, vol. 68, pp. 545–549, 1980.

[35] R. Fairbrother, A. Dolinar, and S. Liu, "Linear and non-linear acoustic modelling of plug flow mufflers," *International Congress on Sound and Vibration*, vol. 15, 2008.

[36] Z. Tao and A. Seybert, "A review of current techniques for measuring muffler transmission loss," *Society of Automotive Engineers, Inc.*, 2001.

[37] H. K. Versteeg and W. Malalasekera, *An introduction to Computational Fluid Dynamics, The Finite Volume Method*. 1995.

[38] M. Chapman, "Flows in internal combustion engines," *The winter annual meeting of the American society of mechanical engineers*, November 1982.

[39] Y. Guo, "Experimental investigation of acoustic properties of mufflers with perforated pipes," *ACC Acoustic Competence Centre*, p. 74, 2007.

[40] L. Rayleigh, *The Theory of Sound II*. McMillan, London, 1894.

[41] U. Ingard, "On the theory and design of acoustics resonators," *The Journal of the Acoustical Society of America*, vol. 25, 1953.

[42] Rschevkin, "Hochfrequenztechnik und elektroakustik," *Hochfrequenztechnik und Elektroakustik*, vol. 67, 1959.

[43] M. Heckl and H. A. Müller, *Taschenbuch der Technischen Akustik*. Springer, 1995.

[44] T. Morel, J. Morel, and D. A. Blaser, "Fluid dynamic and acoustic modeling of concentric-tube resonators/silencers," *SAE Technical Paper Series*, vol. February 25-March 1, 1991.